

Multi-centre normative brain mapping of intracranial EEG lifespan patterns in the human brain

Heather Woodhouse¹, Gerard Hall¹, Callum Simpson¹, Csaba Kozma¹,

Frances Turner¹, Gabrielle M. Schroeder^{1,O}, Beate Diehl³, John S. Duncan³,

Jiajie Mo⁴, Kai Zhang⁴, Aswin Chari⁵, Martin Tisdall⁵, Friederike Moeller⁵,

Chris Petkov^{2,6}, Matthew A. Howard⁶, George M. Ibrahim⁷, Elizabeth Donner⁷,

Nebras M. Warsi⁷, Raheel Ahmed⁸, Peter N. Taylor^{1,2,3}, Yujiang Wang^{1,2,3*}

1. CNNP Lab (www.cnnp-lab.com), Interdisciplinary Computing and Complex BioSystems Group, School of Computing, Newcastle University, Newcastle upon Tyne, United Kingdom
2. Faculty of Medical Sciences, Newcastle University, Newcastle upon Tyne, United Kingdom
3. UCL Queen Square Institute of Neurology, Queen Square, London, United Kingdom
4. Beijing Tiantan Hospital, Beijing, China
5. Great Ormond Street Hospital for Children, London, United Kingdom
6. University of Iowa Hospitals and Clinics, Iowa City, IA, United States
7. The Hospital for Sick Children, University of Toronto, Toronto, Canada
8. University of Wisconsin-Madison, Madison, WI, United States

* Yujiang.Wang@newcastle.ac.uk

^O G.M.S. ORCID ID: 0000-0003-2278-5227

Abstract

Background: Understanding healthy human brain function is crucial to identify and map pathological tissue within it. Whilst previous studies have mapped intracranial EEG (icEEG) from non-epileptogenic brain regions, these maps do not consider the effects of age and sex. Further, most existing work on icEEG has often suffered from a small sample size due to the modality's invasive nature. Here, we substantially increase the subject sample size compared to existing literature, to create a multi-centre, normative map of brain activity which additionally considers the effects of age, sex and recording hospital.

Methods: Using interictal icEEG recordings from $n = 502$ subjects originating from 15 centres, we constructed a normative map of non-pathological brain activity by regressing age and sex on relative band power in five frequency bands, whilst accounting for the hospital effect.

Results: Recording hospital significantly impacted normative icEEG maps in all frequency bands, and age was a more influential predictor of band power than sex. The age effect varied by frequency band, but no spatial patterns were observed at the region-specific level. Certainty about regression coefficients was also frequency band specific and moderately impacted by sample size.

Conclusion: The concept of a normative map is well-established in neuroscience research and particularly relevant to the icEEG modality, which does not allow healthy control baselines. Our key results regarding the hospital site and age effect guide future work utilising normative maps in icEEG.

KEYWORDS: intracranial EEG, normative modelling, lifespan patterns, sex differences, hospital effects, band power

1 Introduction

Age and sex are important factors which are known to influence brain activity. Understanding *how* these variables affect the brain is important for both clinical applications and academic research. Using scalp EEG recordings in children and adolescents, past studies found that age has a negative relationship with relative power in slower frequency bands, namely δ and θ , but a positive relationship with faster ones (α , β) (Clarke et al., 2001; Gasser et al., 1988). Both MEG and scalp EEG studies report some sex differences in the same age range, with males tending to have more α -power (Clarke et al., 2001; Ott et al., 2021). A study in MEG across the whole lifespan found similar frequency band-specific relationships between age and power, whilst a young adult study in scalp EEG reported various sex differences during the resting state (Cave and Barry, 2021; Gómez et al., 2013). In summary, whilst consistent effects across the lifespan have been reported, a conclusive map does not currently exist for electrical brain activity as it does for structural neuroimaging (Bethlehem et al., 2022).

Although much work has been done to assess the impact of age and sex on MRI, MEG and scalp EEG, to our knowledge intracranial EEG (icEEG) has not yet been investigated in this context, most likely because its invasive nature precludes data collection from healthy controls (Cam-CAN et al., 2014; Coffey et al., 1998; Gomez et al., 2017; Hinault et al., 2022). To overcome this issue, researchers have collected icEEG recordings from individuals with epilepsy, from brain regions that were later deemed not pathological and not epileptogenic. By combining these recordings over many individuals, a map of normative brain activity has been proposed (Frauscher et al., 2018a; Groppe et al., 2013; Taylor et al., 2022). Whilst there has been exciting research into normative maps using icEEG and their potential for epilepsy research, the effect of age and sex on icEEG has not been determined (Bernabei et al., 2022; Frauscher et al., 2018a; Kalamangalam et al., 2020; Taylor et al., 2022; Wang et al., 2023).

To analyse this effect thoroughly, this investigation utilises a large data set, encompassing multiple international hospitals. This is similar to Bethlehem et al. (2022) which leverages MRI scans from various studies globally to create brain charts for the human lifespan – our study seeks to help establish such methods in the icEEG literature. Importantly, we will perform our analysis

on the largest multi-centre normative icEEG dataset to date ($n = 502$ subjects), accounting for hospital site effects in data by using mixed-effect modelling. Following this, we aim to uncover and discuss the relationships, if any, between band power extracted from icEEG recordings, and the variables age, sex and recording hospital.

Ultimately, we highlight the need to account for the heterogeneity of icEEG data. We seek to fill a gap in the literature regarding the effect of two standard covariates – age and sex – on band power values extracted from icEEG and modelled in a normative setting. We also expand on previous sample sizes and properly consider hospital variability. Such research is necessary, as an understanding of ageing patterns, sex differences and hospital variation in this modality will conceivably aid in the identification of pathological activity through deviations from ‘normal’ trends.

2 Methods

2.1 Subjects

Our analysis involved 502 individuals with epilepsy undergoing presurgical evaluation with icEEG to localise the seizure onset zone. Data was collected from Beijing Tiantan Hospital, Great Ormond Street Hospital, University of Iowa Hospital, SickKids, University College London Hospital and the University of Wisconsin-Madison. We also used nine hospitals from the publicly available RAM data set (<https://memory.psych.upenn.edu/RAM>), bringing our total number of contributing hospital sites to 15.

Anonymised icEEG recordings were analysed following approval of the Newcastle University Ethics Committee (reference number 23973/2022). Both grid and depth electrode recordings were included. A summary of our final cohort is provided in Figure 1.

2.2 Electrode localisation

For every participant, electrode contacts were localised to regions of interest (ROIs) according to a predefined parcellation, using the “Lausanne scale 36” atlas, with 82 ROIs (Hagmann et al.,

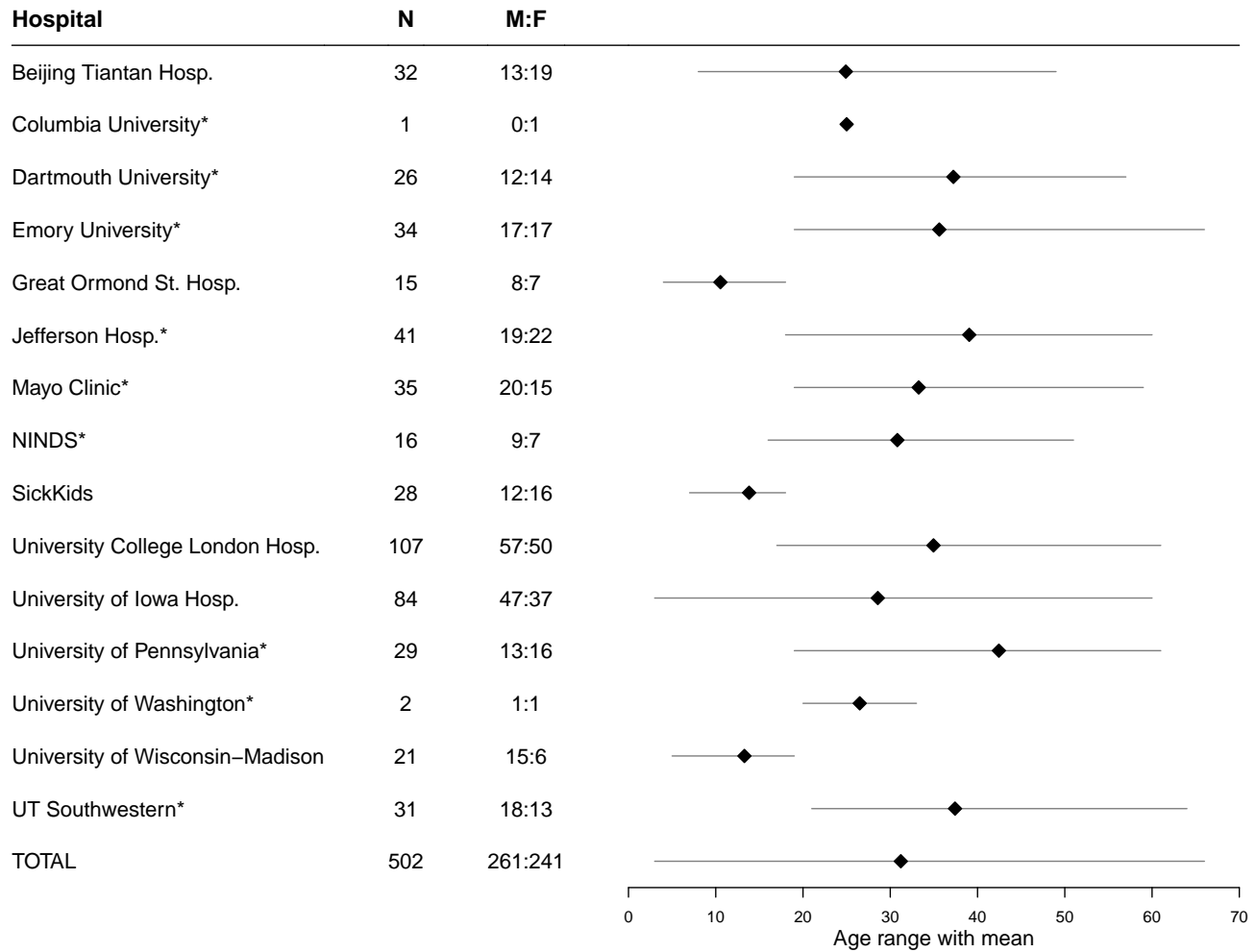


Figure 1: The number of subjects from each participating hospital, along with age and sex distributions. Hospitals from the RAM cohort are highlighted with an *.

2008). The Lausanne atlas has been used previously for normative intracranial analysis (Betz et al., 2019; Taylor et al., 2022).

The methods for localising the electrode contacts to brain regions have also been described previously (Hamilton et al., 2017; Taylor et al., 2022; Wang et al., 2020, 2023). Different hospital sites provided different levels of data, so our methods for localising electrode contacts to ROIs varied between them. Hospitals either provided contact locations in MNI space, or provided native space imaging and co-localised contacts. In the first case, we assigned electrodes to one of 82 regions from the Lausanne scale 36 atlas (Hagmann et al., 2008). We used FreeSurfer to generate volumetric parcellations of an MNI space template brain (Fischl, 2012; Hagmann et al.,

2008). Each electrode contact was assigned to the closest grey matter volumetric region within 5 mm. If the closest grey matter region was >5 mm away then the contact was excluded from further analysis. For the latter case, a similar technique was used, but applied in native space using the subject’s own parcellated pre-operative MRI.

To ensure our findings were robust to parcellation choice, we confirmed that key results held using a finer-grained parcellation (Supplementary S3).

2.3 icEEG processing

Segment selection

For each subject, we extracted a 70-second interictal icEEG segment from a period of relaxed wakefulness, at least two hours away from any detected ictal events. The raw signals and the power spectral densities were visually and algorithmically inspected for spikes, artefacts and faulty channels (see Supplementary S1 for details). Using clinical reports (if available) we excluded any contacts that were: within known lesions, within the seizure onset zone, or subsequently resected. This ensured that at the subject level, we only retained channels thought to be non-pathological in terms of both location in the brain and the signal produced.

If unavailable in clinical reports, information on resected contacts could also be obtained by drawing masks using post- and pre-operative scans (where available), as in Taylor et al. (2022) and Wang et al. (2020). Supplementary S2 details the exclusionary information available for each hospital.

Signal processing

All segments were bandpass filtered between 0.5-80 Hz and downsampled to 200 Hz with an anti-alias filter. A common average reference was applied to all recordings and the power spectral density was calculated using Welch’s method with a 2-second window and 1-second overlap. The average band power was then calculated in five frequency bands: δ (1-4 Hz), θ (4-8 Hz), α (8-13 Hz), β (13-30 Hz) and γ (30-77.5 Hz).

In the γ -band, data between 47.5-52.5 Hz and 57.5-62.5 Hz were excluded from all hospital

sites, to avoid any power line noise. The γ -band was also capped at 77.5 Hz due to 80 Hz noise in the RAM cohort. Band power estimates were \log_{10} transformed and normalised to sum to one in each contact (L1-normalised). These final values are used throughout results to represent relative band power, denoted $\text{RBP}(\cdot)$.

2.4 Normative data table creation

At this stage, the electrode contacts from each subject have been assigned to a single, nearest ROI and the $\text{RBP}(\cdot)$ in five frequency bands has been computed. If multiple contacts from one subject were assigned to the same ROI, then the $\text{RBP}(\cdot)$ values in each frequency band were averaged across contacts to obtain single values of $\text{RBP}(\cdot)$ per region per subject.

We excluded six sub-cortical regions due to no, or a very low number of samples: pallidum, thalamus and accumbens area in both hemispheres, reducing our total number of ROIs from 82 to 76. All cortical regions were retained.

Previous work has demonstrated a left/right symmetry in $\text{RBP}(\cdot)$ in EEG, MEG, and icEEG (Janiukstyte et al., 2023; Owen et al., 2023b; Taylor et al., 2022). Hence, to maximise the number of subjects in each region, we created a ‘mirrored’ version of our data table, in which, the data from homologous regions were combined (e.g., the left amygdala and the right amygdala). In the case of bilateral implantation of symmetric regions, we ensured individuals only had one value of $\text{RBP}(\cdot)$ per ROI and frequency band. This mirrored data table only comprised 38 regions but had markedly more subjects in each. Throughout the results, it will be made clear whether the mirrored (regional), or original (whole-brain), normative data table is in use at any given time.

We confirm the validity of this mirroring in Supplementary S4 by repeating one of our key results using the original data. Additionally, Supplementary S5 demonstrates that our normative values are not related to a subject’s age of epilepsy onset, a feature representing pathology. Unfortunately, we do not have the data to check other disorder-specific features, such as drug levels or epilepsy classification.

In summary, our final normative data table included a unique subject identifier, their age and sex, their originating hospital, and, for the regions in which they had electrode implantation only,

their $RBP(\cdot)$ in five frequency bands averaged across contacts where necessary.

2.5 Statistical modelling and testing

The final step was to fit a suitable model to the normative data to examine the effect of age, sex and hospital site on relative band power. Visual inspection of scatter plots of the $RBP(\cdot)$ values against age in each frequency band (at the whole-brain level) showed no evidence of a non-linear relationship (see Supplementary S6). Further, the effect of having multiple recording hospitals had to be considered, especially as some hospitals supplied only paediatric, or only adult recordings. Therefore, we implemented a linear mixed model (LMM) in each frequency band, specifically a random intercept model, with the originating hospital site as a random effect. Our cohort has a wide range of subjects per hospital (Figure 1), but one of the strengths of mixed modelling is the ability to handle unequal group sizes (West et al., 2014).

Possible fixed effects were age and sex, meaning four LMMs were under consideration in each frequency band:

$$\mathbf{Null: } RBP(\cdot) \sim (1|Hospital)$$

$$\mathbf{Age: } RBP(\cdot) \sim Age + (1|Hospital)$$

$$\mathbf{Sex: } RBP(\cdot) \sim Sex + (1|Hospital)$$

$$\mathbf{Full: } RBP(\cdot) \sim Age + Sex + (1|Hospital)$$

An interaction term between age and sex was also considered but deemed unnecessary (Supplementary S7). Model fitting could be performed at either the regional or whole-brain level. Taking the latter, we calculated several model evaluation statistics to determine the optimal fixed effect structure of the LMM in each frequency band. Since we worked at the whole-brain level, the original data table was used. The statistics under consideration were the AIC and BIC for each model, 95% profiled confidence intervals for the regression coefficients of fixed effects in all but the null model (which has none) and the likelihood ratio test p -values for every pair of models which differed by one variable.

In four frequency bands, each metric was in agreement regarding the optimal LMM, so no further tests were required. The preferred models were the age model in the δ and β bands; the sex model in γ and the full model in θ . The α band demonstrated some uncertainty between the age model and the full model. Since both models perform similarly, we retain the simpler age model as the optimal choice in the α band.

Hence, the optimal LMM was frequency band-specific in our cohort, and so we report frequency band-specific effects throughout our results. We have provided a brief visual overview of our methods (Figure 2). In the results section, we explore both random (hospital site) and fixed (age, sex) effects. Specifically, we investigate if the variables explain $\text{RBP}(\cdot)$ variation, and examine how they might influence it.

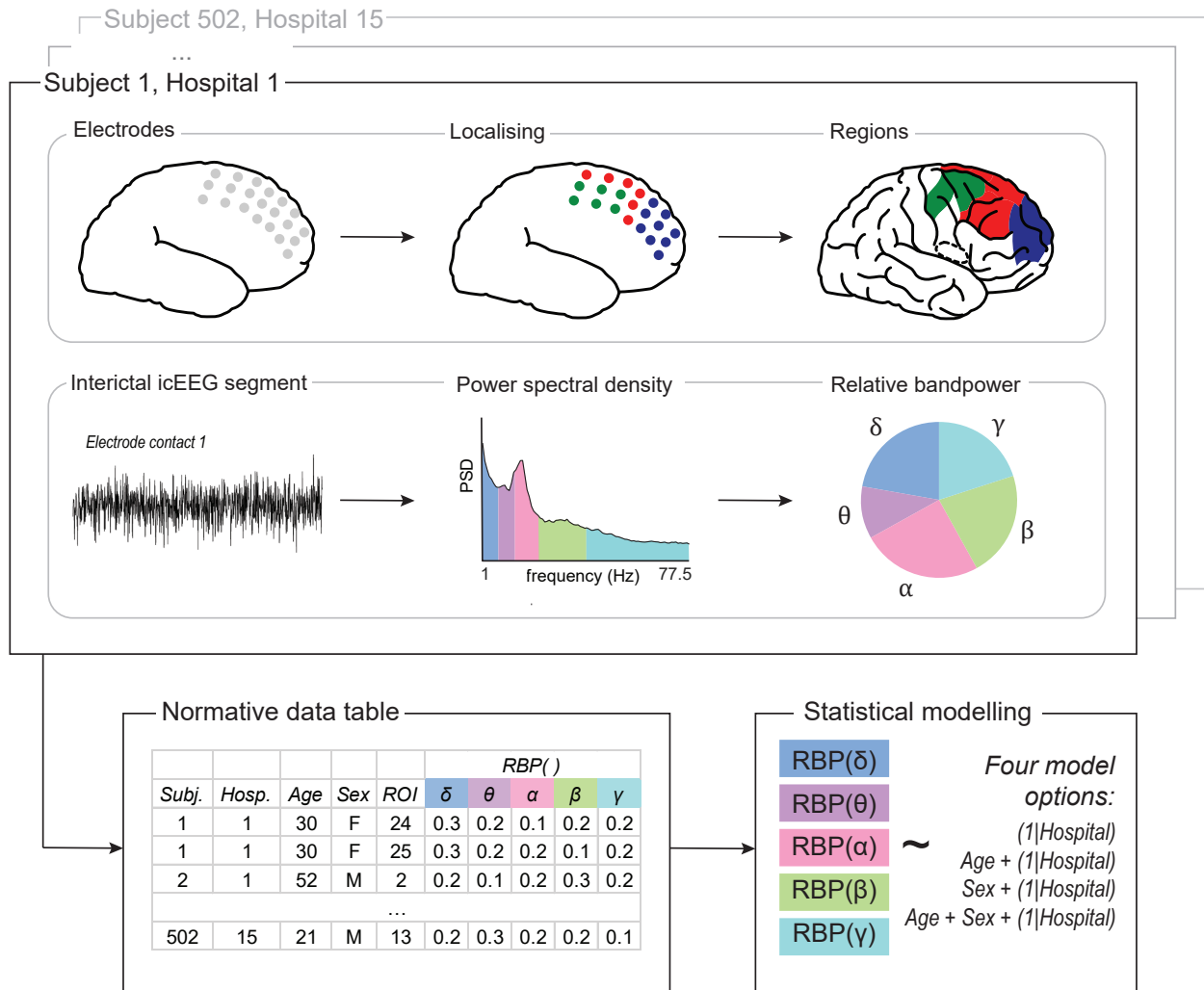


Figure 2: A visual representation of our methods: electrode localisation (top) and signal processing following segment selection (middle), for each subject. Subjects were combined to create our normative data table, to which we applied our statistical models (bottom). All components show dummy data for example purposes only. Brain plots from Scholtens et al. (2021).

3 Results

Results 3.1, 3.2 and 3.3 examine LMMs at the whole-brain level, using the original data. Subsequent results additionally consider the regional-level analysis, and therefore incorporate the mirrored data, to determine if any spatial variations are present in our findings.

3.1 Hospital site effects impacted icEEG normative maps

Focusing first on the random effect structure (recording hospital), we found that in our cohort and model, the hospital site effect was much more powerful in explaining RBP(\cdot) differences at the whole-brain level than any fixed effect structure, in almost all cases. Table 1 quantifies this, showing marginal R^2 values (R_m^2) and intraclass correlation coefficients (ICC) as percentages for the full model, the age model and the sex model. The R_m^2 represents the proportion of variation in RBP(\cdot) explained by the fixed effect(s) of that model. The ICC represents the proportion of the variance explained by the recording hospitals. The optimal LMM as per Section 2.5 has been highlighted for each frequency band.

Note, the R_m^2 values of the two single fixed effect models do not sum exactly to the R_m^2 of the full model, because the denominator in the calculation of R_m^2 includes the residual variance and therefore changes with each model.

	Full model		Age model		Sex model	
	R_m^2	ICC	R_m^2	ICC	R_m^2	ICC
δ	4.28	15.23	4.27	15.27	0.00	19.42
θ	0.60	15.17	0.23	14.88	0.41	16.25
α	8.04	5.09	7.97	5.13	0.00	5.88
β	2.59	6.58	2.58	6.58	0.00	7.93
γ	0.25	32.59	0.01	32.16	0.24	32.25

Table 1: R_m^2 and ICC values (measured in %) for the full model, the age model and the sex model. R_m^2 represents the proportion of variation in RBP(\cdot) explained by the fixed effect(s) of that model. The ICC represents the proportion of the variance explained by the grouping structure, namely recording hospitals. The optimal covariate subset, as determined by a standard model selection process, is highlighted for each frequency band.

There is striking variation in the magnitude of the hospital site effect on $\text{RBP}(\cdot)$ across signal properties. However the ICC s consistently exceed 5%, indicating that, in our cohort, at least a twentieth of the variation in $\text{RBP}(\cdot)$ was explained by the random effect structure. This proportion sometimes reached as high as 30%, attributing that recording hospital impacted $\text{RBP}(\cdot)$ in all frequency bands. Further, in all bands except α , the ICC was consistently larger than the R_m^2 values across models, with this difference being most notable in the θ and γ bands.

To visualise the effect of the originating hospital on $\text{RBP}(\cdot)$, we fit the age model to all data, then selected three well-populated hospitals with similar age ranges and plotted $\text{RBP}(\delta)$ against age, along with the model fit in Figure 3. Additionally, we identified a 33-year-old male from each of the three hospitals and have provided the first 10 seconds of their processed 70-second icEEG segment. The three subjects had variable numbers of channels, so only the first 50 channels are displayed for comparative purposes. Figure 3 demonstrates that while individuals' icEEG segments may appear similar, the originating hospital introduces underlying differences to relative band power properties. Visualisations for all five frequency bands and all hospitals can be found in Supplementary S8.

3.2 Age and sex explained only some of the variation in relative band power

We next examined our fixed effects at the whole-brain level (R_m^2). Neither age nor sex explained a substantial portion of the variance in the $\text{RBP}(\cdot)$, in any frequency band (Table 1). The largest effect was found in the α -band, where R_m^2 was highest at 8%, which in contrast, is similar to the minimum ICC values at around 5%.

Across fixed effects and frequency bands, all R_m^2 values were below 10%, with over half being less than 1%. This suggests that other factors significantly affect $\text{RBP}(\cdot)$ on the whole-brain level, which are not considered here.

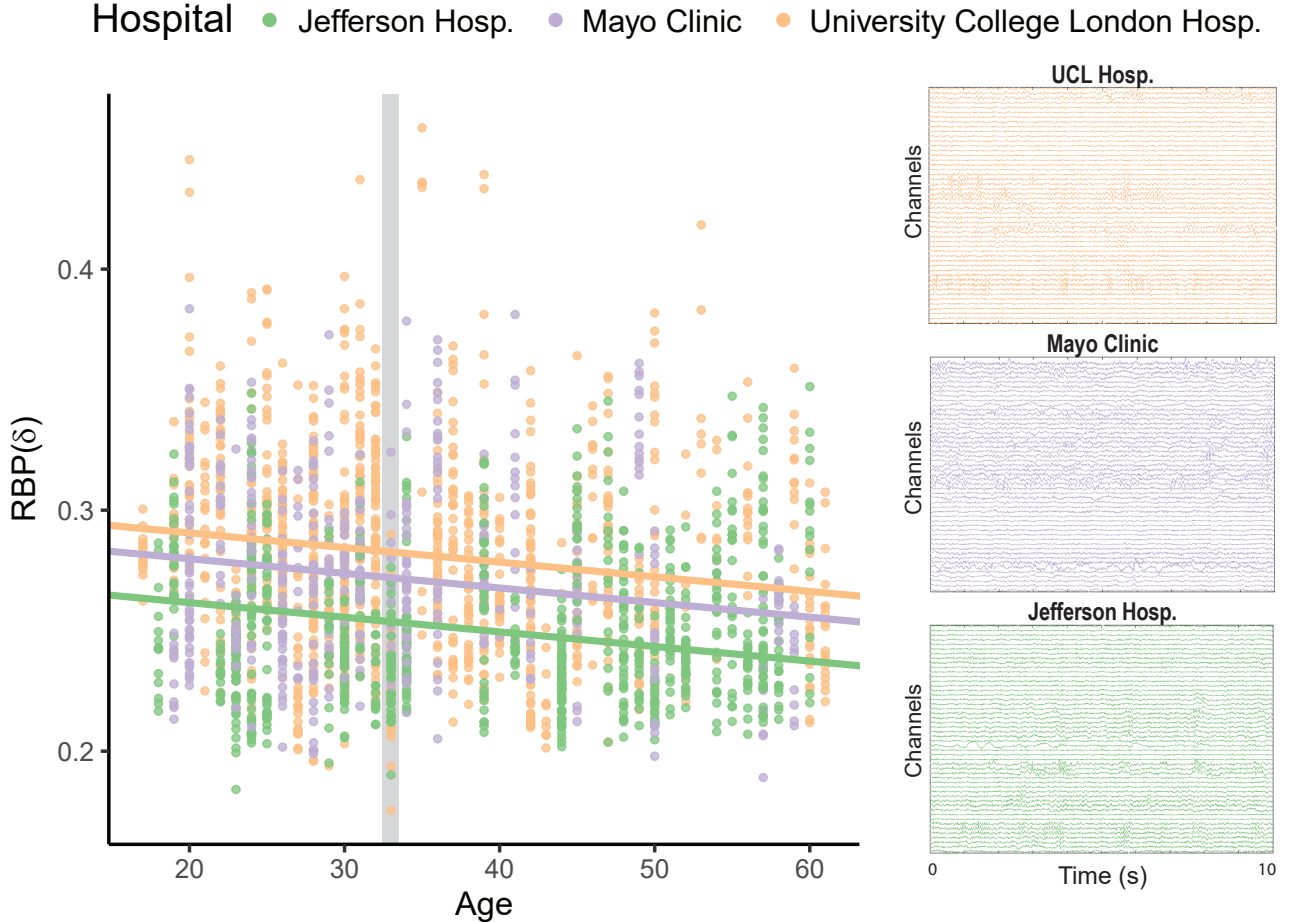


Figure 3: Scatterplot of $RBP(\delta)$ against age for three well-populated hospitals. The age model was implemented for all hospitals, then the age slope and intercepts for Jefferson Hospital, Mayo Clinic and University College London Hospital were extracted and plotted. For three similar individuals, men of age 33, the first 50 channels and 10 seconds of their 70-second preprocessed icEEG segments have been provided. The grey bar indicates where the segments from the 33-year-old men lie within this subset of the data.

3.3 Age was more important than sex for predicting relative band power

Comparing R_m^2 for the age and sex models revealed which of the two was more valuable when predicting $RBP(\cdot)$. All bands which achieve $R_m^2 > 1\%$ do so only when age is included in the model (Table 1). In fact, sex consistently accounted for a negligible portion of the variance in the response, with R_m^2 values below 0.5%. This statement holds even in θ and γ , with sex retained in the optimal LMM, confirming sex was not a significant predictor in this cohort. In contrast, R_m^2 values for age fluctuated notably across frequency bands, being higher in δ , α and β (R_m^2 range of

7.96% and 0.41% for age and sex models respectively).

To validate the lack of sex effect in this cohort, we plotted $\text{RBP}(\cdot)$ against age for all frequency bands at the whole brain level. We then fit the full model and plotted the male/female regression lines. Figure 4 demonstrates visually that sex is not a significant predictor in this cohort, with the differing sex lines being indistinguishable in almost all bands.

Together, Table 1 and Figure 4 emphasize that the influence of sex was minor, and age was the more important predictor of $\text{RBP}(\cdot)$ in our cohort. Hence, subsequent analysis focuses on the age model for all frequency bands; however, we exercise caution when interpreting results in the θ and γ bands, which have a weak relationship with both fixed effects.

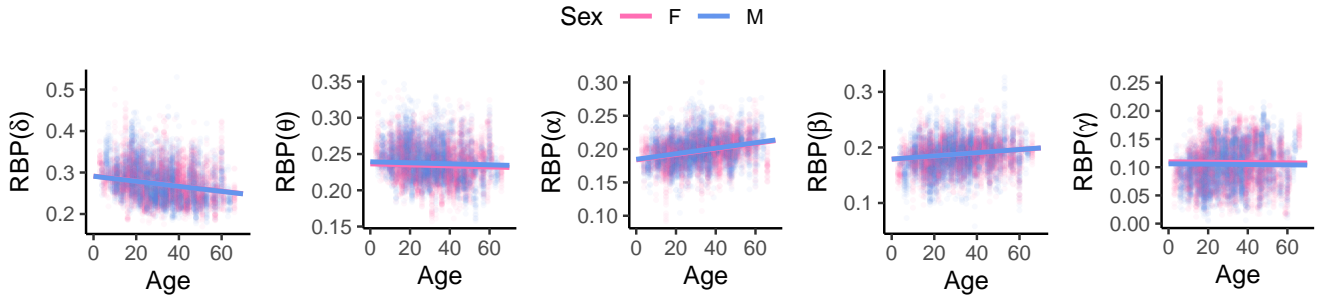


Figure 4: Scatterplots of $\text{RBP}(\cdot)$ against age in every frequency band, using data at the whole-brain level. The full model has been implemented and the male/female regression lines have been plotted.

3.4 The effect of age on band power was spatially uniform and frequency band dependent

With the focus shifted to the age model alone, our goal was to understand *how* age impacted $\text{RBP}(\cdot)$.

Taking the most densely populated ROI (the middle temporal region), the age model was implemented for $\text{RBP}(\cdot)$ in each frequency band and regression coefficients for age (denoted \hat{b}_{age}) were extracted. A visualisation of model fit in this region is provided in Figure 5A, where blue coloured lines indicate that $\text{RBP}(\cdot)$ decreased with age, red lines indicate an increase with age and black lines indicate no relationship (based on 95% confidence intervals for \hat{b}_{age}). This method can be extended to all regions, extracting \hat{b}_{age} for each frequency band and region. The \hat{b}_{age} values

can then be visualised on the brain using a hot/cold colour scale, indicating increasing/decreasing $RBP(\cdot)$ with age (Figure 5B). Finally, disregarding regional information, at the whole-brain level, the age model was implemented in each frequency band and regression coefficients were extracted, along with their 95% confidence intervals (Table 2). Looking at both whole-brain and ROI-level results allowed us to determine if the results had any spatial variation.

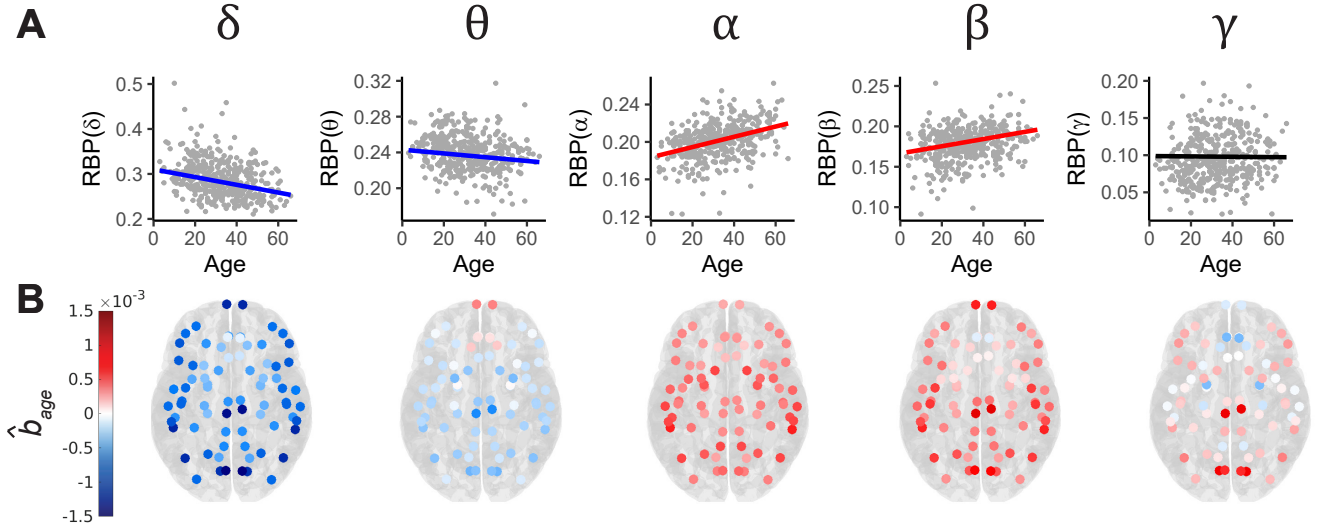


Figure 5: **A)** Visualisations of the age model in each frequency band in the most densely populated region, the middle temporal. Using the 95% confidence intervals for \hat{b}_{age} in the region, blue regression lines indicate a negative relationship between $RBP(\cdot)$ and age, whilst red regression lines indicate a positive one and black indicates no relationship. **B)** Values of \hat{b}_{age} from the age model at the region-level. Values are shown for each ROI and each frequency band of interest. The colour scale is symmetric and fixed across frequency bands with blue representing negative regression coefficients and red representing positive ones. Data from symmetric regions were mirrored, i.e. results are reflected across the midline to provide a whole-brain visualisation.

δ	θ	α	β	γ
-6.1×10^4	-0.8×10^4	4.1×10^4	2.9×10^4	-0.2×10^4
$(-6.7, -5.4) \times 10^4$	$(-1.2, -0.4) \times 10^4$	$(3.8, 4.5) \times 10^4$	$(2.4, 3.3) \times 10^4$	$(-0.7, 0.3) \times 10^4$

Table 2: Values of \hat{b}_{age} along with 95% confidence intervals for each frequency band. Values are rounded to 5 decimal places and were calculated by applying the age model at the whole-brain level.

Opposing relationships between $RBP(\cdot)$ and age were observed at both the region-specific and whole-brain levels, with decreasing trends in δ and θ frequencies, increasing trends in the α and β bands and weaker results found for the γ band.

Figure 5B reveals no discernible spatial gradient in any frequency band, but a clear switch in the sign of \hat{b}_{age} occurs between θ and α , from negative to positive. The θ and γ trends were notably weaker, presenting values of \hat{b}_{age} which are closer to zero, along with some regions deviating from the overarching trends. This is consistent with Table 1 showing that for these two bands, the relationship between age and $\text{RBP}(\cdot)$ is weak, when compared with δ , α and β .

On the whole-brain level, 95% confidence intervals on \hat{b}_{age} reinforced previous results. Table 2 provides no evidence for an age-RBP(γ) relationship and θ 's confidence interval is relatively near zero compared with the remaining three bands. These confidence intervals support the existence of a negative relationship between $\text{RBP}(\delta)$ and age, along with a positive one between $\text{RBP}(\alpha)$ and $\text{RBP}(\beta)$, and age. Hence, the effect of age on $\text{RBP}(\cdot)$ was undoubtedly frequency band-specific in this cohort.

The subset of subjects varies between ROIs in the regional analysis; however, the age distribution in each region did not drive any differences between them (Supplementary S9). The trends in Figure 5B persist in a finer-grained parcellation, and when using the original data in which hemispheres were not mirrored (Supplementary S3 and S4).

3.5 Certainty about age effect was frequency band specific and impacted by sample size

Despite substantial data collection efforts, when analysing region-level models there was an impact of low sample size. Figure 6 displays region-level summaries in every frequency band: the standard error for \hat{b}_{age} , the number of subjects in the region, and a binary indicator of whether or not the 95% confidence interval for \hat{b}_{age} contains 0. It also highlights any regions where the model produced a singular fit.

As a side note, extreme values in Figure 5B co-localise to low sampled regions seen in Figure 6, e.g., the frontal pole stands out from the general trend in θ and only has $n = 38$, highlighting the importance of sample size.

The standard errors revealed that smaller sample sizes can lead to regression coefficient standard errors more than double those of the highly implanted ROIs. However, there appeared to be a

threshold around $n = 150$, beyond which the \hat{b}_{age} standard error lines plateaued, suggesting a lower limit of n , beyond which we can be confident in our findings.

The δ band displayed the highest regression coefficient standard errors almost consistently across ROIs, followed by γ with slightly lower values. Comparatively, α , β and θ bands exhibited lower \hat{b}_{age} standard errors. In regions with approximately $n > 200$, the $SE(\hat{b}_{age})$ values dropped below 0.0002. For α , these same regions consistently showed a regression coefficient standard error of half the size, supporting the positive relationship between $RBP(\alpha)$ and age.

ROI-level confidence intervals also demonstrated that \hat{b}_{age} standard errors varied with frequency band and sample size. Figure 6B shows that in θ and γ bands, regions are dominated by confidence intervals for \hat{b}_{age} that contain 0, whereas the converse is true for δ , α and β .

With the exception of the θ -band, these findings became robust in ROIs with $n \geq 291$. This suggests that equal and large sample sizes in all ROIs may lead to more uniform results and provides further confidence in the relationships we have identified between age and δ , α and β bands, and the lack of one between $RBP(\gamma)$ and age.

The age model returned some singular fits at the regional level (Figure 6B). These regions typically had a low number of data points and a small number of hospitals. We retained all models in all ROIs for completeness.

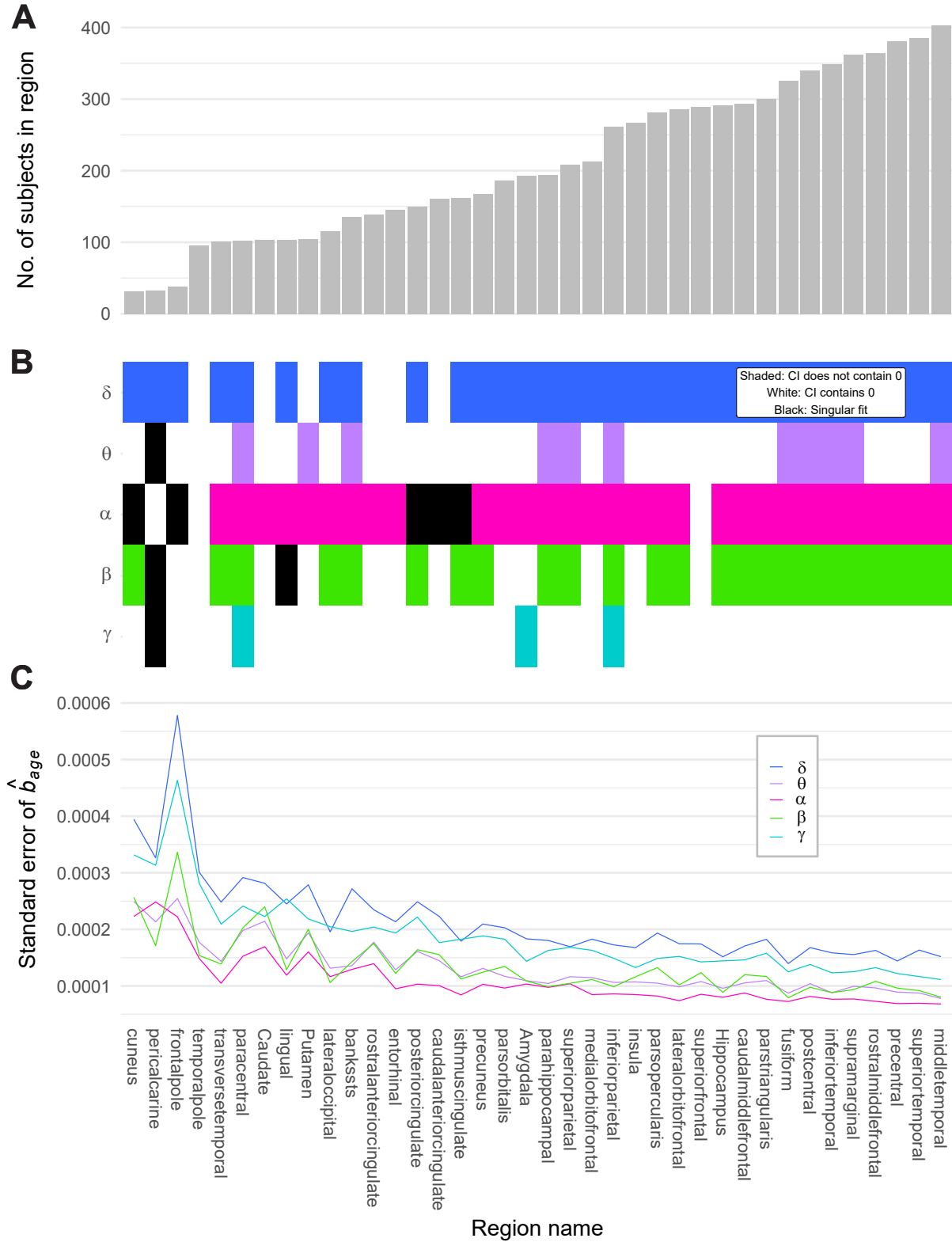


Figure 6: Summaries for each ROI under consideration. The x -axis displays the region name and is ordered by the number of subjects per region. **A)** number of subjects. **B)** a binary indicator of whether the 95% confidence interval for \hat{b}_{age} contains 0 in each frequency band. Singular fits given in black. **C)** standard errors of \hat{b}_{age} in each frequency band.

4 Discussion

In this study, we considered how age, sex, and recording hospital, might impact $\text{RBP}(\cdot)$ in the setting of a normative icEEG map. To understand the effects of the variables, various LMMs were fitted, and it was concluded that sex and $\text{RBP}(\cdot)$ were not related in this cohort, whilst $\text{RBP}(\cdot)$ values present a moderate relationship with subject age and a notable relationship with the recording hospital.

This work provides insight into what the trajectory of $\text{RBP}(\cdot)$ extracted from icEEG might look like in healthy lifespan. Additionally, it confirms that hospital site effects must be considered when modelling multi-centre data, whilst also demonstrating that sex perhaps need not be considered when analysing normative icEEG $\text{RBP}(\cdot)$.

4.1 The relationship between hospital, sex, age and band power

Hospital and band power

In other neuroscience research concerned with normative mapping, such as neuroimaging, the multi-centre problem is widely recognised (Hu et al., 2023; Jovicich et al., 2006; Keshavan et al., 2016). It is common practice to model hospital site effects (or ‘batch’ effects in neuroimaging literature) as random offsets in normative models (Bethlehem et al., 2022; Ge et al., 2024; Hibar et al., 2018; Kim et al., 2022; Little et al., 2024). Whilst it is impossible to capture all sources of hospital (or scanner) heterogeneity, there is some consideration of them in this field. Meanwhile, other neuroscience studies, such as those in EEG, do not typically consider hospital site effects.

For example, the RAM data set involves nine hospitals and is regularly used in academic work to produce results in icEEG (Das et al., 2022; Goldstein et al., 2019; Kozma et al., 2024; Nozari et al., 2023; Taylor et al., 2022; Wang et al., 2023). Whilst the multi-centre challenge here has been recognised before by Miller (2019), to our knowledge, this and other studies have not statistically accounted for the multi-centre structure present. Our work reveals that, in the relative band power properties, the size of the hospital effect is frequency band specific, accounting for up to 30% of the variation.

This demonstrates the necessity of hospital effect consideration, but also raises the question of what drives the differences. Supplementary S8 considers the metadata we have available – electrode type, age range and originating cohort (RAM/other) – as possible contributors to recording hospital differences, but finds no systematic variation in these factors. Other technical aspects could be involved, such as recording settings or electrode manufacturer. Demographic possibilities include race, geography and the hospital’s subject selection criteria.

Whilst both depth and grid/strip electrodes have differing advantages (Taussig et al., 2015), we found no evidence that electrode type was driving recording hospital variation (Supplementary S8). Past work found that both types were efficient for presurgical evaluation, and Frauscher et al. (2018a) do not find any change in spectral density due to electrode type.

Our data did not contain information on subject ethnicity, however, this data should be collected in the future, to address the issue of past exclusionary practices in neuroscience (Li et al., 2022; Ricard et al., 2022). Previous research found race and marital status to be marginally associated with whether or not an individual proceeds to epilepsy surgery (Berg et al., 2003), so it is plausible such factors could also impact whether individuals undergo intracranial examination.

Finally, we wish to highlight the dependency of the hospital site effect size on signal feature in our cohort (Table 1). For example, the hospital site effect was weakest in $RBP(\alpha)$. Investigating whether this is reproducible in other data sets is a further avenue of future research. There may also exist signal features which are more robust towards the effect of recording hospital.

In summary, although the multi-centre effect is under-explored in icEEG research, it is present in our work. Future work should improve on our own by collecting more metadata, to help identify what is driving the hospital site effect and to explain why different signal properties yield different results.

Age and band power

Moving to the fixed effects, our work produced convincing results in the δ , α and β bands when testing for a relationship between $RBP(\cdot)$ and age. Specifically, $RBP(\delta)$ decreased with subject age, while $RBP(\alpha)$ and $RBP(\beta)$ increased. More generally, we found an increase in $RBP(\cdot)$ with

age in fast bands and a decrease in $RBP(\cdot)$ with age in slower bands.

These fixed effect results concur with previous literature on scalp EEG, although here the age range is reduced to children and adolescents, which found fast bands increased and the slow bands decreased in $RBP(\cdot)$ (Clarke et al., 2001; Gasser et al., 1988). Using the same age range, MEG power spectral density maps found an analogous relationship between power and age (Ott et al., 2021).

Looking at the full lifespan (7-84 years) using MEG, previous work found identical trends (a decrease in $RBP(\delta)$ and $RBP(\theta)$, and the converse for higher bands); however, the authors report slight changes around the sixth decade of life (Gómez et al., 2013). Since our maximum age is 18 years less at 66, this result still complements our findings. Further, a study using a small set of scalp electrodes across a large adult cohort found the same age trajectories as ours between 20-40 years, including the strongest decrease being in the δ -band (Hashemi et al., 2016). However, they found that these effects diminished in older age ranges, which our choice of linear modelling does not facilitate.

Finally, there is evidence in the literature of a decrease in alpha band power with age – Tröndle et al. (2023) and Turner et al. (2023) report this across adulthood, and Whitford et al. (2007) in adolescence. However, these studies use absolute power rather than relative, in scalp rather than intracranial EEG, so this does not contradict our findings. Tröndle et al. (2023) also argue that the decrease has been overestimated due to a lack of consideration of the aperiodic component.

Sex and band power

Our work did not find any evidence for a sex- $RBP(\cdot)$ relationship in this cohort. In the literature however, Ott et al. (2021) report sex differences in MEG power spectral density maps for children and adolescents in δ , β and α . They do not report a main effect of sex in θ and γ , which are the same bands in which we found no notable relationship for either fixed effect. Further, Hashemi et al. (2016) report significant sex differences in total band power with age in an adult cohort using scalp EEG.

Nevertheless, as with the evidence for the lifespan decrease in alpha power, both studies use a

different, although related, feature and modality, which may facilitate the sex differences. Finding a difference in absolute power (Hashemi et al., 2016), but not relative power (our cohort) may suggest that the distribution of power is the same for men and women, but that the values differ. Alternatively, it is plausible that there is a genuine effect of sex on $RBP(\cdot)$ but that it is too small to detect in our cohort.

In summary, the age trajectories we have found are generally in line with previous literature in similar areas, but a conclusion on the presence of sex differences remains unclear.

4.2 Existing normative mapping work and how it relates to the ageing patterns

Normative mapping is well-established in neuroscience research showing promising results in a range of modalities including MEG, scalp EEG and icEEG (Frauscher et al., 2018a; Janiukstyte et al., 2023; Niso et al., 2019; Owen et al., 2023b; Taylor et al., 2022). Evidence for the validity of normative maps has been studied, along with their temporal stability (Janiukstyte et al., 2023; Rutherford et al., 2023; Wang et al., 2023). Generally, the patterns noted in neurophysiological normative maps complement each other, indicating their value. For example, many identify well-known trends such as α dominance in parietal and occipital regions (Bosch-Bayard et al., 2020b; Frauscher et al., 2018a; Groppe et al., 2013; Janiukstyte et al., 2023; Owen et al., 2023b; Taylor et al., 2022).

The majority of normative mapping studies outlined consider their maps from a static viewpoint and did not incorporate potential age effects. In this study, we demonstrated that $RBP(\cdot)$ varies with age and that this variation is frequency band-specific. This is not surprising, as there is much previous work evidencing that healthy ageing *does* impact brain activity in modalities such as MEG and scalp EEG (Duffy et al., 1993; Gomez et al., 2017; Gómez et al., 2013). Therefore we suggest, based on our findings, that future work no longer considers icEEG normative maps as a static snapshot and instead strives to incorporate dynamic features, such as age, into any study.

4.3 Clinical potential

Turning now to an application of normative maps, the comparison of individuals with epilepsy (or other disorders) to normalised healthy controls is a common one. It is gaining traction in the field of neurophysiology, using modalities which facilitate said controls such as scalp EEG and MEG (Bosch-Bayard et al., 2020a; Janiukstyte et al., 2023; Owen et al., 2023a,b). Similar work has been produced in the invasive icEEG setting; hence, it is plausible that the ageing trends demonstrated here could yield similar clinical potential (Bernabei et al., 2022; Kozma et al., 2024; Taylor et al., 2022).

Whilst readily interpretable plots such as those in Figure 5B summarise findings well, the core analysis is LMMs fitted at regional (Figures 5A) or whole-brain levels (Table 2). Therefore, to localise pathological tissue in a clinical setting following an icEEG exam, we might compare an individual’s age and $RBP(\cdot)$ in each frequency band to the corresponding regional regression line, quantifying differences, to determine whether their $RBP(\cdot)$ deviates from expected values at that age. Identifying regions with extreme deviations could guide the location of further examination. This particular pipeline would be similar to that suggested in Taylor et al. (2022). In the case of epilepsy, this could complement the standard seizure onset zone localisation techniques following an icEEG exam, without further work or procedures.

4.4 Limitations and future directions

The concept of ‘normative’ data collected from individuals with epilepsy is perhaps contentious. These methods are defensible (Rutherford et al., 2023) and have been applied in previous work (Bernabei et al., 2022; Frauscher et al., 2018a; Kalamangalam et al., 2020; Kozma et al., 2024; Taylor et al., 2022; Wang et al., 2023); however, epilepsy is increasingly defined as a network disorder (Bernhardt et al., 2015; Kramer and Cash, 2012; Rayner and Tailby, 2017), which contrasts with the notion of delineating normal and abnormal tissue. In particular, previous work has shown that more complete resection of seizure onset regions is not associated with more favourable surgical outcomes (Gascoigne et al., 2024). Hence, it is arguable that the icEEG description of pathological tissue is complex and incomplete.

Additionally, sample size impacted results despite our efforts in data collection (Section 3.5), with high regional variation in number of subjects. In an ideal world, we would attain a similar number of subjects per region so they could be more accurately compared. In practice, however, this is not feasible due to some areas being more prone to pathology and therefore being more likely to have electrodes implanted – for example, drug-resistant epilepsies in adults are common in the temporal lobe (Bernhardt et al., 2019).

A further drawback is that our maximum age was only 66 years, so we did not have the full lifespan. This will always be difficult due to the risk of surgical operations on the elderly (Grivas et al., 2006), which limits the ability to directly compare our results to the many other modalities which extend to much older ages (Cam-CAN et al., 2014; Duffy et al., 1993; Gómez et al., 2013; Hashemi et al., 2016). Arguably the minimum age of our cohort (4 years) also does not reflect the full lifespan, however, research has shown that children at younger ages have successfully undergone icEEG-guided epilepsy surgery and tolerated the invasive exam well (Taussig et al., 2016). Future data collection efforts could focus on expanding our age range at both ends.

Similarly, the proportion of paediatric individuals in our cohort is low (Figure 1). In future work, we aim to collect more paediatric recordings and analyse this age range in isolation in an icEEG normative setting. This would provide insight into the effects of ageing during this key stage of life, as previously done for both scalp and MEG (Clarke et al., 2001; Gasser et al., 1988; Gomez et al., 2017; Ott et al., 2021).

Future work might also consider different frequency ranges. This study involves frequency content from 1-77.5 Hz, but higher frequency bands can contain pathological high-frequency oscillations (HFOs), which are thought to delineate epileptogenic tissue (Zweiphenning et al., 2016, 2019). Previous work has provided a normative map for HFOs obtained from icEEG (Frauscher et al., 2018b). Hence, accounting for HFOs as in Kuroda et al. (2021) and extending the frequency range of our normative map could improve its clinical potential for identifying pathological areas of the brain.

A further line of enquiry would be to increase the complexity of the model beyond *linear* mixed models and consider the quadratic case or beyond. This has been done in other modalities, which

found some frequency bands required non-linear models of band power over age, whilst other bands did not (Duffy et al., 1993; Gómez et al., 2013). Future work might investigate whether icEEG trajectories mirror those results, or if perhaps the optimal model complexity is not only frequency band specific, but regionally specific as well.

Combining the discussions around frequency ranges and model complexity, there is also evidence that more granular frequency bands could affect the model selection process. For example, using healthy MEG data to determine how $\text{RBP}(\cdot)$ changes with age, Gómez et al. (2013) found that a linear regression model performed best for $\text{RBP}(\text{low-}\beta)$, but a quadratic model is preferable for $\text{RBP}(\text{high-}\beta)$. Analogous results were found in scalp EEG in the α -band as well as the β -band (more complex models were required for the upper end of the band range) (Gasser et al., 1988).

Different features of EEG could also be considered, in particular, absolute band power as an alternative to the relative band power used here. This would allow for direct comparison to the aforementioned work which finds sex differences in absolute power (Hashemi et al., 2016). However, a previous EEG study investigating age, sex and band power found that absolute power failed to find significant lifespan effects in all bands except δ , whilst relative power succeeded, suggesting further investigation using absolute power is unnecessary (Clarke et al., 2001).

4.5 Conclusions

In conclusion, our results suggest that whilst recording hospital and age have some impact on normative icEEG $\text{RBP}(\cdot)$ in this cohort, sex does not. Our work might be considered the first attempt to study the relationship between these variables and icEEG in a normative setting. Our results highlight the importance of accounting for the heterogeneity in icEEG data by including covariates such as age and recording hospital (where applicable) in future normative mapping work.

Sample size is a key discussion point of this study, being both a strength and limitation of our work. Whilst we have collected one of the largest icEEG datasets to date, some of our results are limited by number of subjects per region. Future work could strive to address this, whilst also considering the impact of non-linear models, or the effects of using a different EEG feature.

We propose that the dynamic nature of normative mapping should be acknowledged in future icEEG research, rather than only considering a static viewpoint that does not account for variables such as age. Further, multi-centre work needs to investigate and model the impact of using data from several recording hospitals to ensure the accurate interpretation of any results.

5 Data and code availability

The preprocessed, normative data table including RBP(\cdot) values, along with code used for modelling and to produce figures, will be made available at <https://github.com/H-Woodhouse/norm-ic EEG-age-sex-hospital> upon acceptance.

The data from RAM hospitals is publicly available at <https://memory.psych.upenn.edu/RAM>. Due to data sharing agreements, the raw icEEG for the remaining hospitals is not available. However, the CNRP lab will be publishing a data release paper containing this in the future.

6 Author Contributions

- Conceptualisation: YW HW
- Methodology: YW HW PNT GMS
- Analysis: HW
- Data Acquisition: HW BD JSD JM KZ AC MT FM CP MAH GMI ED NMW RA PNT YW
- Data processing: HW GH CS CK FT GMS PNT YW
- Writing - Original Draft: HW
- Writing - Review & Editing: HW GMS JSD AC MT FM CP MAH GMI NMW PNT YW
- Supervision: YW

7 Funding

P.N.T. and Y.W. are both supported by UKRI Future Leaders Fellowships (MR/T04294X/1, MR/V026569/1). H.W. and C.S. are supported by the Engineering and Physical Sciences Research Council (EP/L015358/1); J.S.D. is supported by the NIHR UCLH/UCL Biomedical Research Centre. C.K. is supported by Epilepsy Research UK. R.A. is supported by the Clinical and Translational Science Award, Grant UL1TR002373, NIH/NCATS. G.M.I. was funded by the Abe Bresver Chair in Functional Neurosurgery at the Hospital for Sick Children.

8 Declaration of Competing Interests

None of the authors have any conflict of interest to disclose.

9 Acknowledgements

We thank members of the Computational Neurology, Neuroscience & Psychiatry Lab (www.cnnp-lab.com) for discussions on the analysis and manuscript. We thank our coauthors for their data contribution and feedback on the manuscript.

Supplementary Material

S1 Algorithmic detection of noisy or faulty channels

Channels were removed based on the five criteria given below. American hospitals were run separately from the European hospitals and Beijing, due to the line noise difference.

1. Exclude channels based on channel details data. If channels are known to be resected, within structurally abnormal tissue or within the seizure onset zone, they are removed. This is determined by resection masks or clinical reports.
2. Exclude algorithmically detected noisy channels by finding channels with outlier signal range and/or variance relative to the other channels.
 - Two rounds of detection are performed; the first round is before preprocessing with (by default) less stringent detection thresholds, and the second is after basic preprocessing.
 - The first round uses a threshold for outlier detection of 16, for both signal variance and range.
 - Before the second round, common average is applied to the icEEG data.
 - A 4th order band pass filter is applied between 0 and 100 Hz.
 - A notch filter is applied to eliminate the location-specific line noise (50 Hz for European hospitals and Beijing Tiatian Hospital and 60 Hz for American hospitals).
 - The threshold for outlier detection based on signal range and variance in the second round following preprocessing is 12.
3. Exclude channels previously marked as ‘bad’. These are the channels noted as noisy/faulty by visual inspection.
4. Remove channels which are missing channel details.
5. Remove channels without mapping/localisation to an ROI.

S2 Available channel details by hospital site

Three additional channel features were recorded if available through clinical reports or resection masks, namely, whether the channel was 1) within the seizure onset zone, if determined 2) located in structurally abnormal tissues such as lesions or, 3) resected during surgery. If a channel fell into any of these categories, it was removed from analysis. Table S1 demonstrates how many subjects (per hospital site) had these variables in their reports.

	Total subjects	Number of subjects with information on:		
		SOZ	Structural abnormality	Resection
Beijing Tiantan Hosp.	32	32	0	28
Columbia University*	1	1	1	0
Dartmouth University*	26	26	26	0
Emory University*	34	34	34	0
Great Ormond St. Hosp.	15	15	0	13
Jefferson Hosp.*	41	41	41	0
Mayo Clinic*	35	35	35	0
NINDS*	16	16	16	0
SickKids	28	0	0	0
University of Pennsylvania*	29	29	29	0
University College London Hosp.	107	102	0	106
University of Iowa Hosp.	84	22	0	51
University of Washington*	2	2	2	0
University of Wisconsin-Madison	21	21	0	0
UT Southwestern*	31	31	31	0

Table S1: For each hospital site, the number of subjects with information on which electrode contacts are: within SOZs, within structural abnormalities, resected.

S3 Robustness to parcellation choice

Our main results use the coarsest scale parcellation, scale 36, with data mirrored across hemispheres for sample size reasons. Here, we repeat Figure 5B again in a finer-grained parcellation, the scale 60 atlas. Here, the data has *not* been mirrored.

Due to a decrease in sample size per region, more regions produce a singular fit. Using the scale 36 atlas, as shown in Figure 6B, there are a total of 9 singular fits out of 190 total fits (38 ROIs \times 5 bands). When using the scale 60 atlas, without mirroring, there are 61 singular fits out of 610 total fits (122 ROIs \times 5 bands), which is a significantly larger portion – approximately double. This is due to the LMM fitted in each ROI being too complex for the size of the data at this finer-grained parcellation. For this reason, we did not consider any finer-grained atlases.

Nevertheless, as shown in Figure S1, using the scale 60 atlas, results are reasonably symmetric in δ , α and β . Any deviations from symmetry/expected results, tend to lie near the midline, whose regions have lower sample sizes than lateral ones. The θ and γ bands do not exhibit symmetry, but as outlined in Section 3.3, their relationship with age was weak.

We conclude that while (for this cohort) the model under consideration is only suitable for the parcellation applied in the main paper, symmetry holds to a satisfactory level when considering one, finer-grained parcellation.

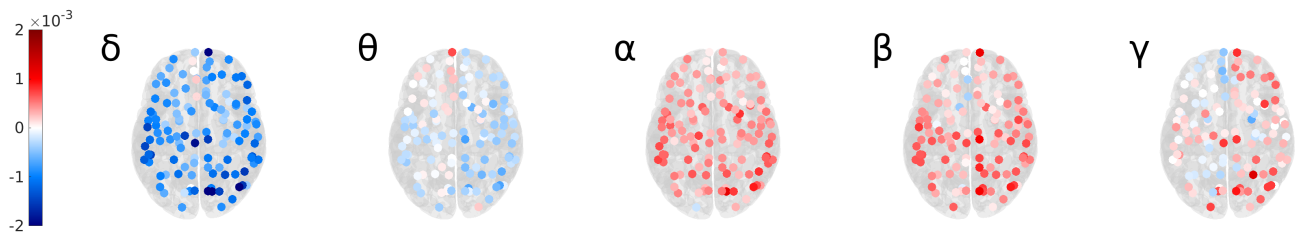


Figure S1: Values of \hat{b}_{age} from the age model implemented at the region-level for the scale 60 atlas. Values are shown for each ROI and each frequency band of interest. The colour scale is symmetric and fixed across frequency bands with blue representing negative regression coefficients and red representing positive ones. The original data has been used so results are not reflected across the midline.

S4 Validity of mirroring data in our parcellation

In Section 2.4 we described the mirroring of symmetric regions in order to increase the sample size in each region. The only instance where we mirror across the midline for visualisation is found in Figure 5B. Here we repeat that figure, without mirroring symmetric regions, to demonstrate that the main results are unchanged. Note that, due to the reduction in sample size per ROI using the full data, there are 28 singular fits, treble the number attained when using mirrored data.

Figure S2 demonstrates that results are symmetric when using the original data in bands where we have identified a relationship between $\text{RBP}(\cdot)$ and age, and the overarching trends are unchanged. We see a decrease in $\text{RBP}(\delta)$ and $\text{RBP}(\theta)$ with age, an increase in $\text{RBP}(\alpha)$ and $\text{RBP}(\beta)$, and weak results for $\text{RBP}(\gamma)$. There is no spatial specificity in the results, and trends are weaker in the θ and γ bands. This is all in line with results presented in Result 3.4.

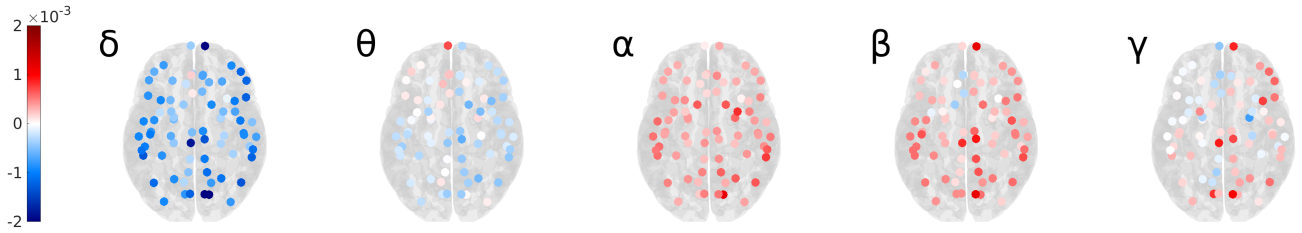


Figure S2: Values of \hat{b}_{age} from the age model implemented at the region-level for the scale 36 atlas. Values are shown for each ROI and each frequency band of interest. The colour scale is symmetric and fixed across frequency bands with blue representing negative regression coefficients and red representing positive ones. The original data has been used so results are not reflected across the midline.

S5 Normative values are not correlated with age of epilepsy onset

After implementing the age model in all frequency bands at the ROI level using the mirrored data, we tested for correlation between model residuals and age of epilepsy onset.

Not every subject has age of onset data, so we fit the age model to all data, then applied Spearman’s test using only complete pairs. Figure S3 shows the absolute value of the correlation estimate in each ROI and frequency band (top). Near-white values demonstrate strong correlation (in either direction) whilst dark red values indicate no, or weak, correlation. The p -value plot

(bottom) on the same axes shows a dark orange when $p < 0.05$. It shows a light orange if the converse is true. The x -axis is ordered from lowest to highest number of subjects per region.

Figure S3 is dominated by low correlations and non-significant p -values, indicating no relationship between age of onset and normative band power values, and further supporting that our data are representative of normative, rather than pathological activity.

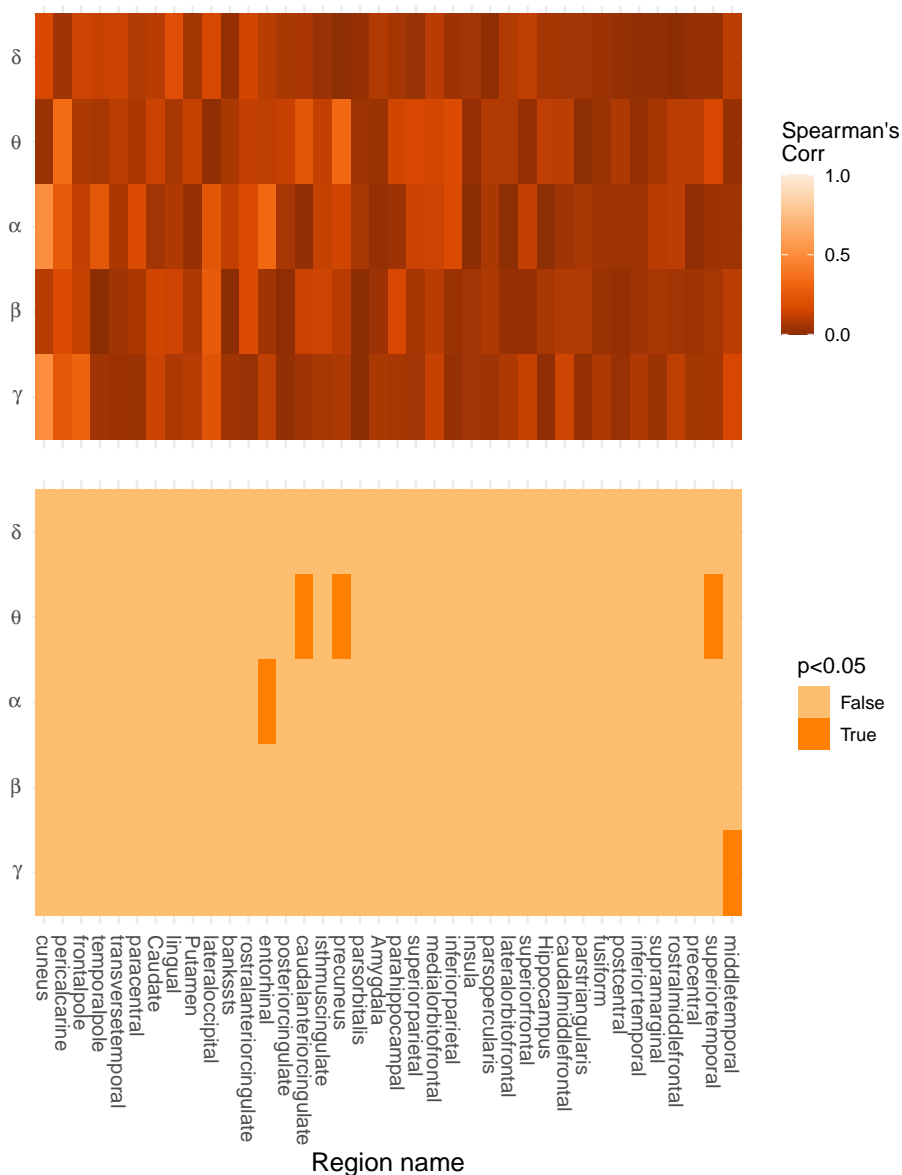


Figure S3: Heatmaps representing Spearman's correlation test applied to the residuals of the age model and age of epilepsy onset, in every frequency band and ROI. Absolute correlation coefficients (top) are on a gradient colour scale with near-white representing high correlation and dark red representing low values. Corresponding p -values (bottom) have a binary indicator of significance at the 5% level. We have not applied a multiple-comparison correction, but the rate of detection is in agreement with and below what would be expected at 5% level (5 detections out of 190 tests). The regions are ordered by number of subjects, from low to high.

S6 No evidence of a non-linear relationship between $\text{RBP}(\cdot)$ and age

We decided a linear mixed model would be suitable for this work (Section 2.5) as we did not see strong evidence that the relationship between $\text{RBP}(\cdot)$ and age was non-linear. Figure S4 shows all data at the whole-brain level, and presents a generally linear trend in each frequency band.

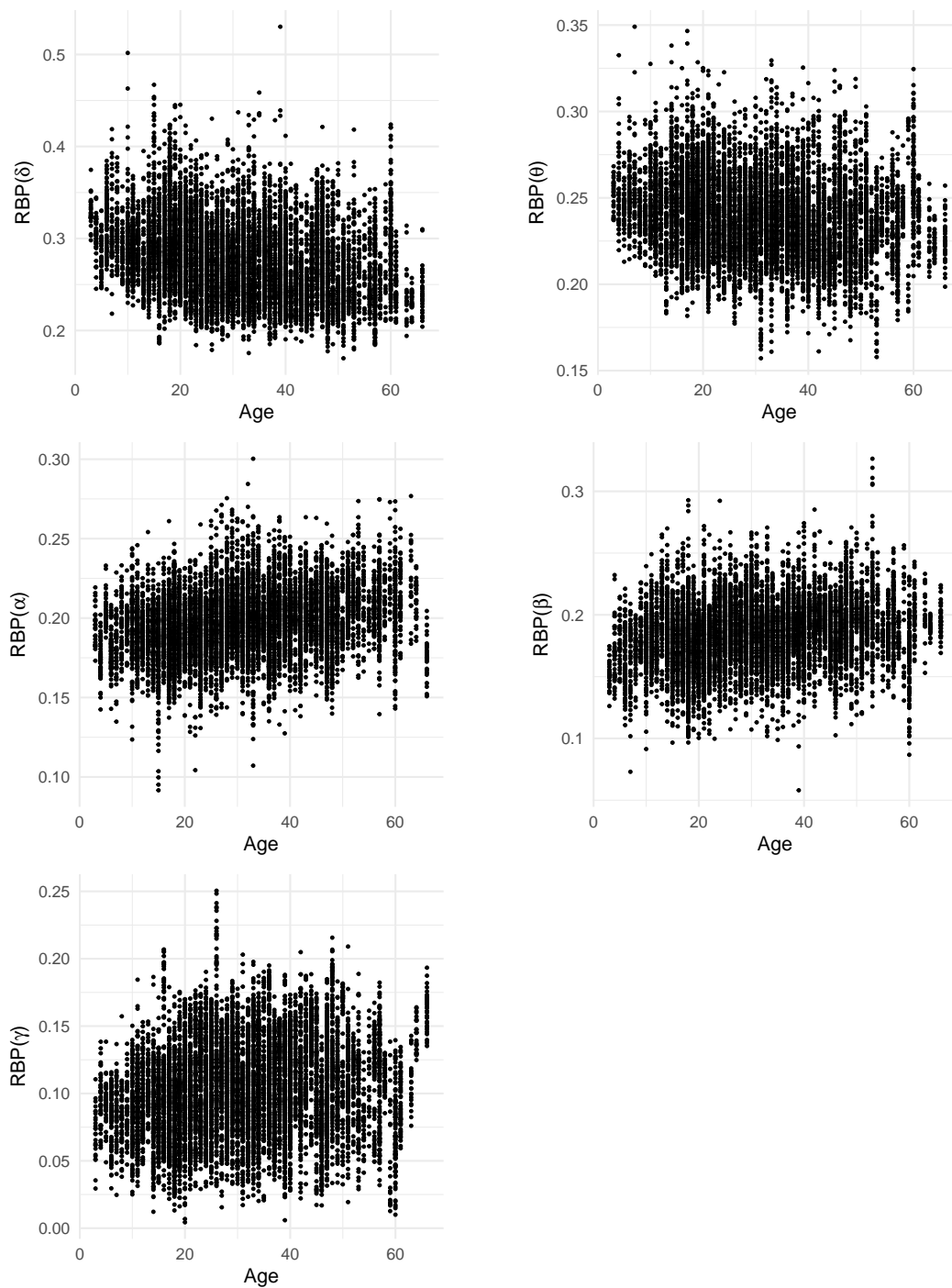


Figure S4: Scatter plots of $\text{RBP}(\cdot)$ against age in each frequency band, using the original data at the whole-brain level

S7 Consideration of an interaction term between age and sex

During the model selection process in Section 2.5, we additionally considered a fifth covariate structure involving an interaction term, giving a final model for each frequency band, $RBP(\cdot) \sim Age + Sex + Age * Sex + (1|Hospital)$.

During the model selection process, δ , β and γ returned non-zero confidence intervals on the interaction term, however, model evaluation statistics did not unanimously select the interaction model, and it performed similarly to the simpler, optimal choice in each case. In the α -band the interaction was not significant. The θ -band selected the interaction model, however as determined throughout our results, $RBP(\theta)$ has a weak relationship with our covariates. For these reasons, we didn't consider the interaction term in the main text.

To demonstrate the lack of value of an interaction term further down the pipeline, we repeat Table 1 here with the interaction model included. Looking at the R_m^2 columns, the inclusion of an interaction term adds a maximum of 0.18% to the variation in $RBP(\cdot)$ explained by our fixed effects structure. In the θ -band where the interaction model is preferred, the response variance explained by fixed effects is $< 1\%$. Hence an interaction term was not considered within our main results.

	Interaction model		Full model		Age model		Sex model	
	R_m^2	ICC	R_m^2	ICC	R_m^2	ICC	R_m^2	ICC
δ	4.46	15.26	4.28	15.23	4.27	15.27	0.00	19.42
θ	0.70	15.10	0.60	15.17	0.23	14.88	0.41	16.25
α	8.07	5.16	8.04	5.09	7.97	5.13	0.00	5.88
β	2.71	6.59	2.59	6.58	2.58	6.58	0.00	7.93
γ	0.37	32.55	0.25	32.59	0.01	32.16	0.24	32.25

Table S2: R_m^2 and ICC values (measured in %) for the interaction model, the full model, the age model and the sex model. R_m^2 represents the proportion of variation in $RBP(\cdot)$ explained by the fixed effect(s) of that model. The ICC represents the proportion of the variance explained by the grouping structure, namely recording hospitals. The optimal covariate subset, as determined by a standard model selection process, is highlighted for each frequency band.

S8 Hospital site effects across all frequency bands and hospitals

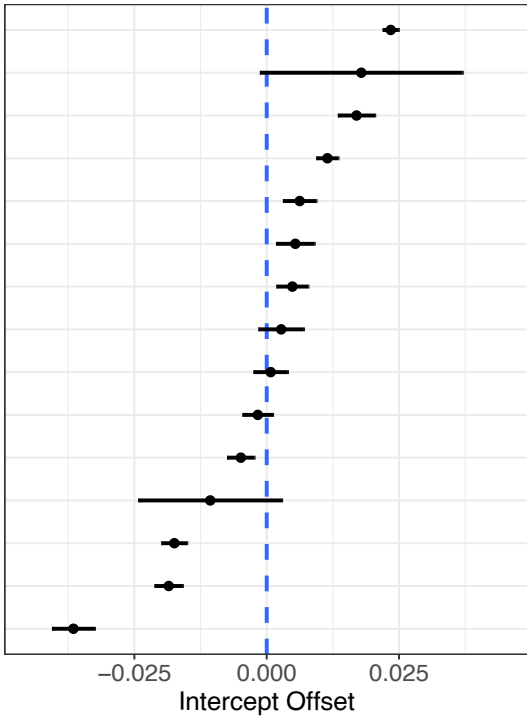
In Figure 3, we used one frequency band and three hospitals to demonstrate the hospital effect visually, overlaid on the normative data points. Here, we fit the age model on the whole brain level to demonstrate the varying hospital intercepts across all hospital sites and frequency bands, to highlight the importance of the consideration of such effects.

Figure S5 shows (for each frequency band) the deviation of each hospital’s intercept from the population intercept, along with a standard 95% confidence interval. In other words, each hospital’s deviation from the mean population $RBP(\cdot)$. Additionally, metadata has been included on the left of the plot, indicating which hospitals originated from the RAM database, which hospitals used only depth electrodes, and which hospitals had only paediatric, or only adult subjects. On the y -axis, hospitals are ordered by deviation from the overarching intercept in that band. The x -axis range is fixed across figures, demonstrating how some frequency bands show greater variation across recording hospitals.

Columbia University and the University of Washington consistently display notably large confidence intervals as a result of their low sample size. Whilst some hospitals fall above or below population means in each band, there are no hospitals which are systematically different across all five subplots. Further, there are no groupings, such as only paediatric hospitals, which show a consistent pattern across signal properties.

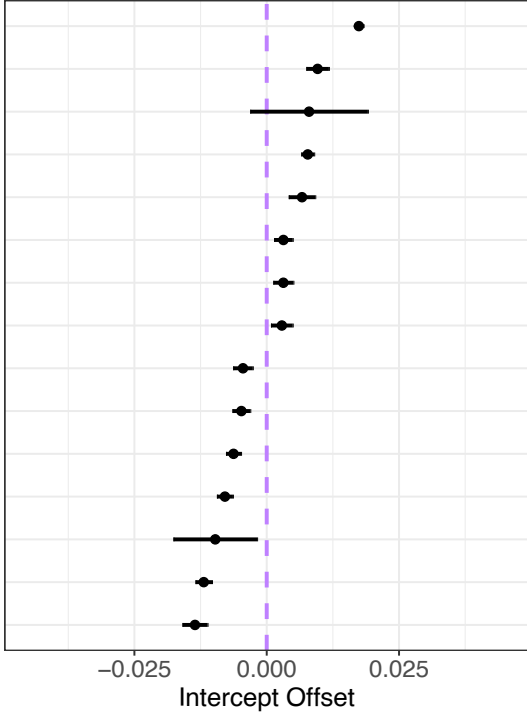
Hence, we do not have sufficient metadata to determine what is driving the large, varied hospital site effects, it does not appear to be any of the variables present in our cohort. Further investigation is required to determine the source of the recording hospital differences in $RBP(\cdot)$.

University of Iowa Hosp.	Other	Full	All
Columbia University	RAM	Adult	Depth only
Beijing Tiantan Hosp.	Other	Full	Depth only
University College London Hosp.	Other	Adult	All
Dartmouth University	RAM	Adult	All
University of Wisconsin–Madison	Other	Paediatric	All
SickKids	Other	Paediatric	All
Great Ormond St. Hosp.	Other	Paediatric	Depth only
Mayo Clinic	RAM	Adult	All
University of Pennsylvania	RAM	Adult	All
Emory University	RAM	Adult	All
University of Washington	RAM	Adult	All
Jefferson Hosp.	RAM	Adult	All
UT Southwestern	RAM	Adult	All
NINDS	RAM	Adult	All



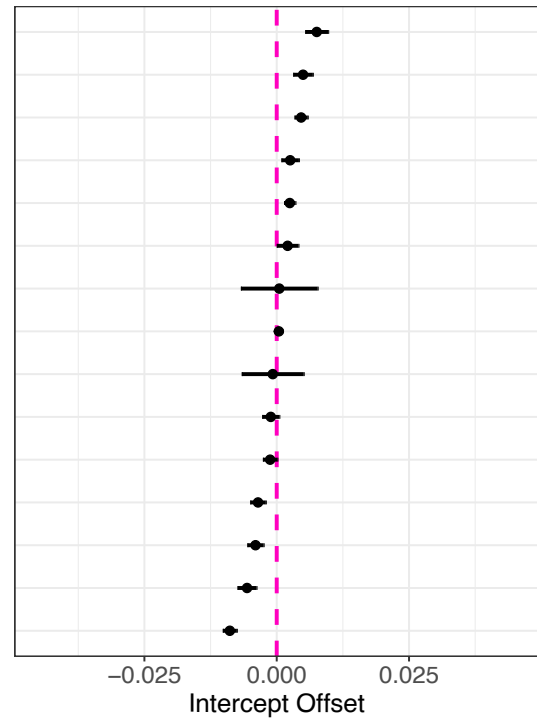
(a) δ -band

University of Iowa Hosp.	Other	Full	All
University of Wisconsin–Madison	Other	Paediatric	All
Columbia University	RAM	Adult	Depth only
University College London Hosp.	Other	Adult	All
Great Ormond St. Hosp.	Other	Paediatric	Depth only
SickKids	Other	Paediatric	All
Mayo Clinic	RAM	Adult	All
Beijing Tiantan Hosp.	Other	Full	Depth only
Dartmouth University	RAM	Adult	All
University of Pennsylvania	RAM	Adult	All
Jefferson Hosp.	RAM	Adult	All
Emory University	RAM	Adult	All
University of Washington	RAM	Adult	All
UT Southwestern	RAM	Adult	All
NINDS	RAM	Adult	All



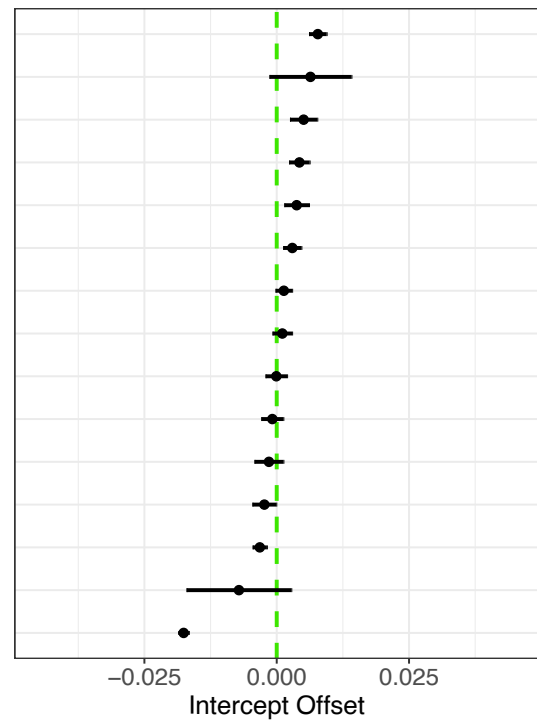
(b) θ -band

Great Ormond St. Hosp.	Other	Paediatric	Depth only
University of Wisconsin–Madison	Other	Paediatric	All
Jefferson Hosp.	RAM	Adult	All
Mayo Clinic	RAM	Adult	All
University College London Hosp.	Other	Adult	All
NINDS	RAM	Adult	All
Columbia University	RAM	Adult	Depth only
University of Iowa Hosp.	Other	Full	All
University of Washington	RAM	Adult	All
Dartmouth University	RAM	Adult	All
UT Southwestern	RAM	Adult	All
University of Pennsylvania	RAM	Adult	All
SickKids	Other	Paediatric	All
Beijing Tiantan Hosp.	Other	Full	Depth only
Emory University	RAM	Adult	All

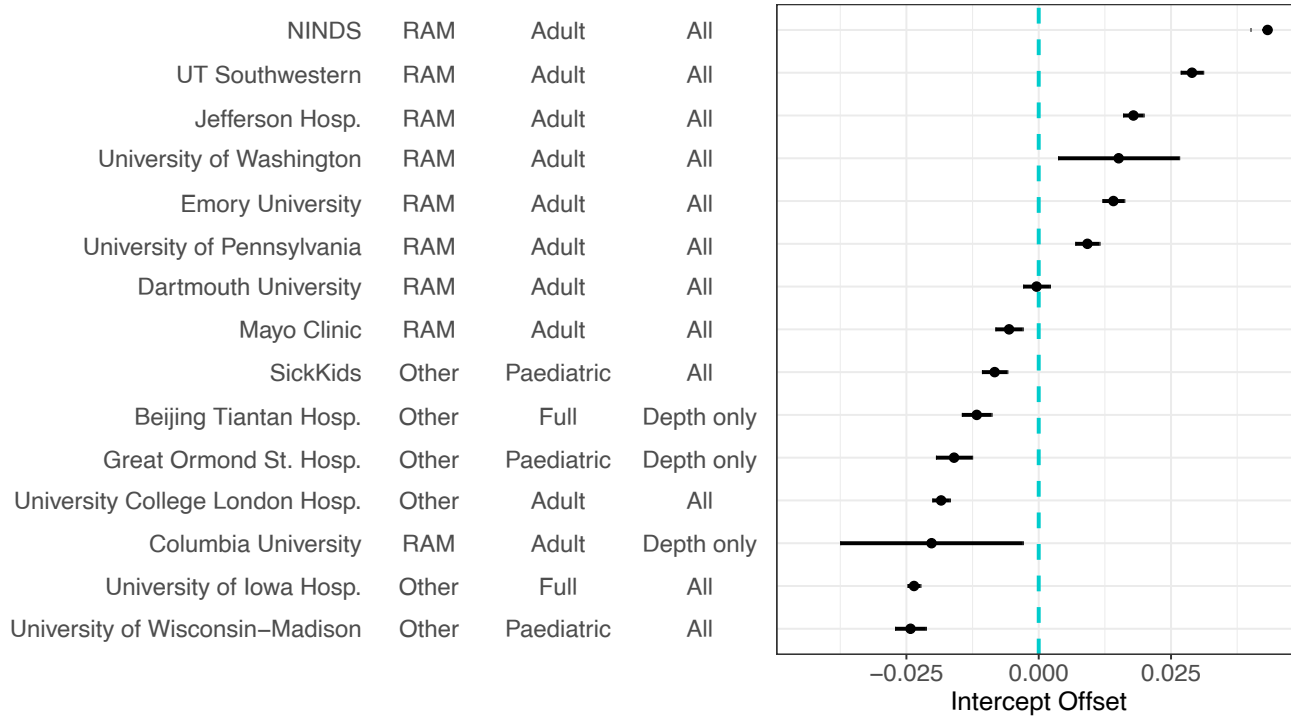


(c) α -band

Emory University	RAM	Adult	All
University of Washington	RAM	Adult	All
NINDS	RAM	Adult	All
SickKids	Other	Paediatric	All
University of Wisconsin–Madison	Other	Paediatric	All
UT Southwestern	RAM	Adult	All
Jefferson Hosp.	RAM	Adult	All
University of Pennsylvania	RAM	Adult	All
Dartmouth University	RAM	Adult	All
Mayo Clinic	RAM	Adult	All
Great Ormond St. Hosp.	Other	Paediatric	Depth only
Beijing Tiantan Hosp.	Other	Full	Depth only
University College London Hosp.	Other	Adult	All
Columbia University	RAM	Adult	Depth only
University of Iowa Hosp.	Other	Full	All



(d) β -band



(e) γ -band

Figure S5: For each frequency band **a)-e)**: Plots showing each recording hospital’s deviation from the population intercept when fitting the age model at the whole brain level. The x -axis is fixed at a range of $(-0.05, 0.05)$ for all bands. The hospitals are ordered on the y -axis by largest positive offset from the $RBP(\cdot)$ population mean, to largest negative offset. Three metadata columns on the left of the plot show three grouping variables. Namely 1) if the hospital originated from the RAM dataset, 2) if the hospital comprises only paediatric subjects, only adults, or the full age range, 3) if the retained subjects from the hospital had only depth electrode implantation, or whether there were some individuals with grid/strip electrodes as well.

S9 Age distributions at ROI-level

Results 3.4 and 3.5, employ the age model at the regional level. Whilst we discuss the number of subjects per model, this could be misleading in this context if, for example, a highly populated ROI only consisted of a very narrow age range. Such a scenario would undoubtedly impact any results surrounding \hat{b}_{age} .

Hence, we have calculated the 2.5th and 97.5th percentiles to give the 95% central age range in each region, and plotted this against the regions \hat{b}_{age} value. This has been repeated for all five frequency bands and the result can be seen in Figure S6.

All ROIs have a minimum 2.5-97.5th percentile age range of 43 years, with about half the

regions reaching 50 years or more. Additionally, in all five frequency bands, there is no correlation between \hat{b}_{age} and the distribution of ages, as confirmed by Spearman's method. Therefore, there is a reasonable distribution of subject ages in each ROI, and there is no evidence that this distribution is influencing regional results. It is acceptable to discuss sample size of regions as the influencing factor in the relevant results.

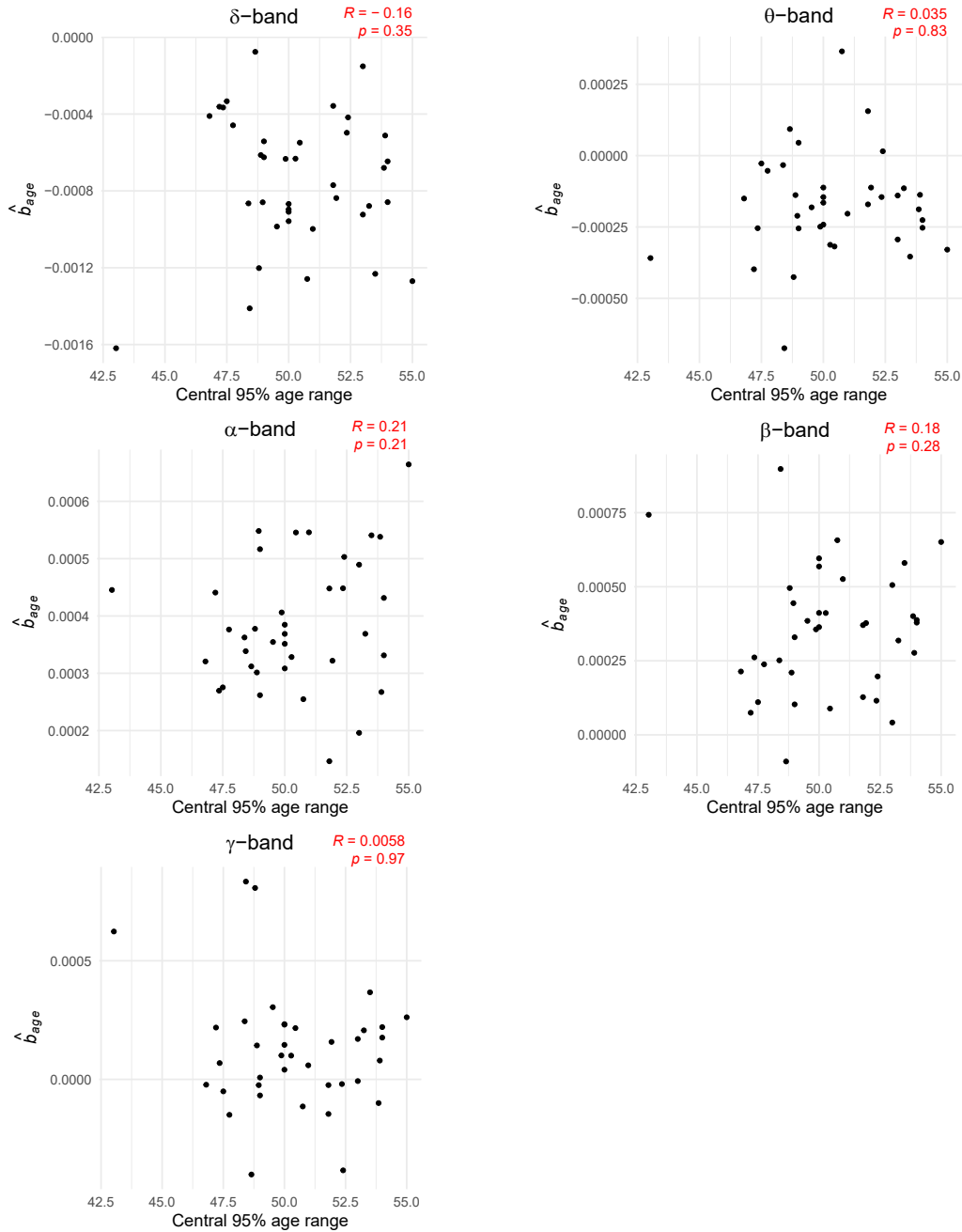


Figure S6: Values of \hat{b}_{age} from the age model implemented at the region-level for the scale 36 atlas plotted against the central 95% percentile range of subject ages in that region. Results are given for all frequency bands with Spearman's correlation coefficient and resulting p -value in the top-right corner.

References

- Anne T Berg, Barbara G Vickrey, John T Langfitt, Michael R Sperling, Thaddeus S Walczak, Shlomo Shinnar, Carl W Bazil, Steven V Pacia, Susan S Spencer, and Multicenter Study of Epilepsy Surgery. The multicenter study of epilepsy surgery: recruitment and selection for surgery. *Epilepsia*, 44(11):1425–1433, November 2003.
- John M Bernabei, Nishant Sinha, T Campbell Arnold, Erin Conrad, Ian Ong, Akash R Pattnaik, Joel M Stein, Russell T Shinohara, Timothy H Lucas, Dani S Bassett, Kathryn A Davis, and Brian Litt. Normative intracranial EEG maps epileptogenic tissues in focal epilepsy. *Brain*, 145(6):1949–1961, 05 2022. ISSN 0006-8950. doi: 10.1093/brain/awab480. URL <https://doi.org/10.1093/brain/awab480>.
- Boris C Bernhardt, Leonardo Bonilha, and Donald W Gross. Network analysis for a network disorder: The emerging role of graph theory in the study of epilepsy. *Epilepsy Behav.*, 50: 162–170, September 2015.
- Boris C Bernhardt, Fatemeh Fadaie, Min Liu, Benoit Caldairou, Shi Gu, Elizabeth Jefferies, Jonathan Smallwood, Danielle S Bassett, Andrea Bernasconi, and Neda Bernasconi. Temporal lobe epilepsy. *Neurology*, 92(19):e2209–e2220, May 2019.
- R A I Bethlehem, J Seidlitz, S R White, J W Vogel, K M Anderson, C Adamson, S Adler, G S Alexopoulos, E Anagnostou, A Areces-Gonzalez, D E Astle, B Auyeung, M Ayub, J Bae, G Ball, S Baron-Cohen, R Beare, S A Bedford, V Benegal, F Beyer, J Blangero, M Blesa Cábez, J P Boardman, M Borzage, J F Bosch-Bayard, N Bourke, V D Calhoun, M M Chakravarty, C Chen, C Chertavian, G Chetelat, Y S Chong, J H Cole, A Corvin, M Costantino, E Courchesne, F Crivello, V L Cropley, J Crosbie, N Crossley, M Delarue, R Delorme, S Desrivieres, G A Devenyi, M A Di Biase, R Dolan, K A Donald, G Donohoe, K Dunlop, A D Edwards, J T Elison, C T Ellis, J A Elman, L Eyler, D A Fair, E Feczko, P C Fletcher, P Fonagy, C E Franz, L Galan-Garcia, A Gholipour, J Giedd, J H Gilmore, D C Glahn, I M Goodyer, P E Grant, N A Groenewold, F M Gunning, R E Gur, R C Gur, C F Hammill, O Hansson, T Hedden, A Heinz,

R N Henson, K Heuer, J Hoare, B Holla, A J Holmes, R Holt, H Huang, K Im, J Ipser, C R Jack, Jr, A P Jackowski, T Jia, K A Johnson, P B Jones, D T Jones, R S Kahn, H Karlsson, L Karlsson, R Kawashima, E A Kelley, S Kern, K W Kim, M G Kitzbichler, W S Kremen, F Lalonde, B Landeau, S Lee, J Lerch, J D Lewis, J Li, W Liao, C Liston, M V Lombardo, J Lv, C Lynch, T T Mallard, M Marcelis, R D Markello, S R Mathias, B Mazoyer, P McGuire, M J Meaney, A Mechelli, N Medic, B Misic, S E Morgan, D Mothersill, J Nigg, M Q W Ong, C Ortinau, R Ossenkoppele, M Ouyang, L Palaniyappan, L Paly, P M Pan, C Pantelis, M M Park, T Paus, Z Pausova, D Paz-Linares, A Pichet Binette, K Pierce, X Qian, J Qiu, A Qiu, A Raznahan, T Rittman, A Rodrigue, C K Rollins, R Romero-Garcia, L Ronan, M D Rosenberg, D H Rowitch, G A Salum, T D Satterthwaite, H L Schaare, R J Schachar, A P Schultz, G Schumann, M Schöll, D Sharp, R T Shinohara, I Skoog, C D Smyser, R A Sperling, D J Stein, A Stolicyn, J Suckling, G Sullivan, Y Taki, B Thyreau, R Toro, N Traut, K A Tsvetanov, N B Turk-Browne, J J Tuulari, C Tzourio, É Vachon-Preseu, M J Valdes-Sosa, P A Valdes-Sosa, S L Valk, T van Amelsvoort, S N Vandekar, L Vasung, L W Victoria, S Villeneuve, A Villringer, P E Vértes, K Wagstyl, Y S Wang, S K Warfield, V Warriar, E Westman, M L Westwater, H C Whalley, A V Witte, N Yang, B Yeo, H Yun, A Zalesky, H J Zar, A Zettergren, J H Zhou, H Ziauddeen, A Zugman, X N Zuo, 3R-BRAIN, AIBL, Alzheimer’s Disease Neuroimaging Initiative, Alzheimer’s Disease Repository Without Borders Investigators, CALM Team, Cam-CAN, CCNP, COBRE, cVEDA, ENIGMA Developmental Brain Age Working Group, Developing Human Connectome Project, FinnBrain, Harvard Aging Brain Study, IMAGEN, KNE96, Mayo Clinic Study of Aging, NSPN, POND, PREVENT-AD Research Group, VETSA, E T Bullmore, and A F Alexander-Bloch. Brain charts for the human lifespan. *Nature*, 604(7906):525–533, April 2022.

Richard Betzel, John Medaglia, Ari Kahn, Jonathan Soffer, Daniel Schonhaut, and Danielle Bassett. Structural, geometric and genetic factors predict interregional brain connectivity patterns probed by electrocorticography. *Nature Biomedical Engineering*, 3:1, 11 2019. doi: 10.1038/s41551-019-0404-5.

Jorge Bosch-Bayard, Eduardo Aubert-Vazquez, Shawn T. Brown, Christine Rogers, Gregory Kiar, Tristan Glatard, Lalet Scaria, Lidice Galan-Garcia, Maria L. Bringas-Vega, Trinidad Virues-

Alba, Armin Taheri, Samir Das, Cecile Madjar, Zia Mohaddes, Leigh MacIntyre, CHBMP , Alan C. Evans, and Pedro A. Valdes-Sosa. A quantitative eeg toolbox for the mni neuroinformatics ecosystem: Normative spm of eeg source spectra. *Frontiers in Neuroinformatics*, 14, 2020a. ISSN 1662-5196. doi: 10.3389/fninf.2020.00033. URL <https://www.frontiersin.org/articles/10.3389/fninf.2020.00033>.

Jorge Bosch-Bayard, Lidice Galan, Eduardo Aubert Vazquez, Trinidad Virues Alba, and Pedro A. Valdes-Sosa. Resting state healthy eeg: The first wave of the cuban normative database. *Frontiers in Neuroscience*, 14, 2020b. ISSN 1662-453X. doi: 10.3389/fnins.2020.555119. URL <https://www.frontiersin.org/articles/10.3389/fnins.2020.555119>.

Cam-CAN, Meredith A. Shafto, Lorraine K. Tyler, Marie Dixon, Jason R. Taylor, James B. Rowe, Rhodri Cusack, Andrew J. Calder, William D. Marslen-Wilson, John Duncan, Tim Dalgleish, Richard N. Henson, Carol Brayne, Ed Bullmore, Karen Campbell, Teresa Cheung, Simon Davis, Linda Geerligs, Rogier Kievit, Anna McCarrey, Darren Price, David Samu, Matthias Treder, Kamen Tsvetanov, Nitin Williams, Lauren Bates, Tina Emery, Sharon Erzinçlioglu, Andrew Gadie, Sofia Gerbase, Stanimira Georgieva, Claire Hanley, Beth Parkin, David Troy, Jodie Allen, Gillian Amery, Liana Amunts, Anne Barcroft, Amanda Castle, Cheryl Dias, Jonathan Dowrick, Melissa Fair, Hayley Fisher, Anna Goulding, Adarsh Grewal, Geoff Hale, Andrew Hilton, Frances Johnson, Patricia Johnston, Thea Kavanagh-Williamson, and Magdalena Kwasniewska. The cambridge centre for ageing and neuroscience (cam-can) study protocol: A cross-sectional, lifespan, multidisciplinary examination of healthy cognitive ageing. *BMC Neurology*, 14(1), 2014. ISSN 1471-2377. doi: 10.1186/s12883-014-0204-1. Publisher Copyright: © 2014 Shafto et al.

Adele E. Cave and Robert J. Barry. Sex differences in resting eeg in healthy young adults. *International Journal of Psychophysiology*, 161:35–43, 2021. ISSN 0167-8760. doi: <https://doi.org/10.1016/j.ijpsycho.2021.01.008>. URL <https://www.sciencedirect.com/science/article/pii/S0167876021000209>.

Adam R Clarke, Robert J Barry, Rory McCarthy, and Mark Selikowitz. Age and sex effects in the eeg: development of the normal child. *Clinical Neurophysiology*, 112(5):806–814, 2001.

ISSN 1388-2457. doi: [https://doi.org/10.1016/S1388-2457\(01\)00488-6](https://doi.org/10.1016/S1388-2457(01)00488-6). URL <https://www.sciencedirect.com/science/article/pii/S1388245701004886>.

C. Edward Coffey, Joseph F. Lucke, Judith A. Saxton, Graham Ratcliff, Lori Jo Unitas, Brenda Billig, and R. Nick Bryan. Sex Differences in Brain Aging: A Quantitative Magnetic Resonance Imaging Study. *Archives of Neurology*, 55(2):169–179, 02 1998. ISSN 0003-9942. doi: 10.1001/archneur.55.2.169. URL <https://doi.org/10.1001/archneur.55.2.169>.

Anup Das, Carlo de Los Angeles, and Vinod Menon. Electrophysiological foundations of the human default-mode network revealed by intracranial-EEG recordings during resting-state and cognition. *Neuroimage*, 250(118927):118927, April 2022.

Frank H. Duffy, Gloria B. McAnulty, and Marilyn S. Albert. The pattern of age-related differences in electrophysiological activity of healthy males and females. *Neurobiology of Aging*, 14(1):73–84, 1993. ISSN 0197-4580. doi: [https://doi.org/10.1016/0197-4580\(93\)90025-7](https://doi.org/10.1016/0197-4580(93)90025-7). URL <https://www.sciencedirect.com/science/article/pii/0197458093900257>.

Bruce Fischl. Freesurfer. *NeuroImage*, 62(2):774–781, 2012. ISSN 1053-8119. doi: <https://doi.org/10.1016/j.neuroimage.2012.01.021>. URL <https://www.sciencedirect.com/science/article/pii/S1053811912000389>. 20 YEARS OF fMRI.

Birgit Frauscher, Nicolas von Ellenrieder, Rina Zelman, Irena Doležalová, Lorella Minotti, André Olivier, Jeffery Hall, Hoffmann Dominique, Nguyen Dang Khoa, Philippe Kahane, François Dubeau, and Jean Gotman. Atlas of the normal intracranial electroencephalogram: Neurophysiological awake activity in different cortical areas. *Brain : a journal of neurology*, 141, 03 2018a. doi: 10.1093/brain/awy035.

Birgit Frauscher, Nicolás von Ellenrieder, Rina Zelman, Christine Rogers, Dang Khoa Nguyen, Philippe Kahane, François Dubeau, and Jean Gotman. High-frequency oscillations in the normal human brain. *Ann. Neurol.*, July 2018b.

Sarah J. Gascoigne, Nathan Evans, Gerard Hall, Csaba Kozma, Mariella Panagiotopoulou, Gabrielle M. Schroeder, Callum Simpson, Christopher Thornton, Frances Turner, Heather

Woodhouse, Jess Blickwedel, Fahmida A. Chowdhury, Beate Diehl, John S. Duncan, Ryan Faulder, Rhys H. Thomas, Kevin Wilson, Peter N. Taylor, and Yujiang Wang. Incomplete resection of the intracranial electroencephalographic seizure onset zone is not associated with postsurgical outcomes. *Epilepsia*, July 2024. ISSN 1528-1167. doi: 10.1111/epi.18061. URL <http://dx.doi.org/10.1111/epi.18061>.

Theo Gasser, Rolf Verleger, Petra Bächer, and Lothar Sroka. Development of the eeg of school-age children and adolescents. i. analysis of band power. *Electroencephalography and Clinical Neurophysiology*, 69(2):91–99, 1988. ISSN 0013-4694. doi: [https://doi.org/10.1016/0013-4694\(88\)90204-0](https://doi.org/10.1016/0013-4694(88)90204-0). URL <https://www.sciencedirect.com/science/article/pii/0013469488902040>.

Ruiyang Ge, Yuetong Yu, Yi Xuan Qi, Yu-Nan Fan, Shiyu Chen, Chuntong Gao, Shalaila S Haas, Faye New, Dorret I Boomsma, Henry Brodaty, Rachel M Brouwer, Randy Buckner, Xavier Caseras, Fabrice Crivello, Eveline A Crone, Susanne Erk, Simon E Fisher, Barbara Franke, David C Glahn, Udo Dannlowski, Dominik Grotegerd, Oliver Gruber, Hilleke E Hulshoff Pol, Gunter Schumann, Christian K Tamnes, Henrik Walter, Lara M Wierenga, Neda Jahanshad, Paul M Thompson, Sophia Frangou, and ENIGMA Lifespan Working Group. Normative modelling of brain morphometry across the lifespan with CentileBrain: algorithm benchmarking and model optimisation. *Lancet Digit. Health*, 6(3):e211–e221, March 2024.

Hannah E. Goldstein, Elliot H. Smith, Robert E. Gross, Barbara C. Jobst, Bradley C. Lega, Michael R. Sperling, Gregory A. Worrell, Kareem A. Zaghloul, Paul A. Wanda, Michael J. Kahana, Daniel S. Rizzuto, Catherine A. Schevon, Guy M. McKhann, and Sameer A. Sheth. Risk of seizures induced by intracranial research stimulation: Analysis of 770 stimulation sessions. *Journal of neural engineering*, 16(6), November 2019. ISSN 1741-2560. doi: 10.1088/1741-2552/ab4365. Publisher Copyright: © 2019 IOP Publishing Ltd.

Carlos Gomez, Elena Rodríguez-Martínez, Fernando Maestú, Jesús Poza, and Carlos Gómez. Absolute power spectral density changes in the magnetoencephalographic activity during the transition from childhood to adulthood. *Brain Topography*, 30, 01 2017. doi: 10.1007/s10548-016-0532-0.

- Athanasios Grivas, Johannes Schramm, Thomas Kral, Marec Von Lehe, Christoph Helmstaedter, Christian E. Elger, and Hans Clusmann. Surgical treatment for refractory temporal lobe epilepsy in the elderly: Seizure outcome and neuropsychological sequels compared with a younger cohort. *Epilepsia*, 47(8):1364–1372, 2006. doi: <https://doi.org/10.1111/j.1528-1167.2006.00608.x>. URL <https://onlinelibrary.wiley.com/doi/abs/10.1111/j.1528-1167.2006.00608.x>.
- David M. Groppe, Stephan Bickel, Corey J. Keller, Sanjay K. Jain, Sean T. Hwang, Cynthia Harden, and Ashesh D. Mehta. Dominant frequencies of resting human brain activity as measured by the electrocorticogram. *NeuroImage*, 79:223–233, 2013. ISSN 1053-8119. doi: <https://doi.org/10.1016/j.neuroimage.2013.04.044>. URL <https://www.sciencedirect.com/science/article/pii/S1053811913003911>.
- Carlos Gómez, Jose M Pérez-Macías, Jesús Poza, Alberto Fernández, and Roberto Hornero. Spectral changes in spontaneous meg activity across the lifespan. *Journal of Neural Engineering*, 10(6):066006, oct 2013. doi: [10.1088/1741-2560/10/6/066006](https://doi.org/10.1088/1741-2560/10/6/066006). URL <https://dx.doi.org/10.1088/1741-2560/10/6/066006>.
- Patric Hagmann, Leila Cammoun, Xavier Gigandet, Reto Meuli, Christopher Honey, Van Wedeen, and Olaf Sporns. Mapping the structural core of human cerebral cortex. *PLoS biology*, 6:e159, 08 2008. doi: [10.1371/journal.pbio.0060159](https://doi.org/10.1371/journal.pbio.0060159).
- Liberty S Hamilton, David L Chang, Morgan B Lee, and Edward F Chang. Semi-automated anatomical labeling and inter-subject warping of high-density intracranial recording electrodes in electrocorticography. *Frontiers in Neuroinformatics*, 11:62, 2017.
- Ali Hashemi, Lou J. Pino, Graeme Moffat, Karen J. Mathewson, Chris Aimone, Patrick J. Bennett, Louis A. Schmidt, and Allison B. Sekuler. Characterizing population eeg dynamics throughout adulthood. *eNeuro*, 3(6), 2016. doi: [10.1523/ENEURO.0275-16.2016](https://doi.org/10.1523/ENEURO.0275-16.2016). URL <https://www.eneuro.org/content/3/6/ENEURO.0275-16.2016>.
- D P Hibar, for the ENIGMA Bipolar Disorder Working Group, L T Westlye, N T Doan, N Jahanshad, J W Cheung, C R K Ching, A Versace, A C Bilderbeck, A Uhlmann, B Mwangi, B Krämer,

B Overs, C B Hartberg, C Abé, D Dima, D Grotegerd, E Sprooten, E Bøen, E Jimenez, F M Howells, G Delvecchio, H Temmingh, J Starke, J R C Almeida, J M Goikolea, J Houenou, L M Beard, L Rauer, L Abramovic, M Bonnin, M F Ponteduro, M Keil, M M Rive, N Yao, N Yalin, P Najt, P G Rosa, R Redlich, S Trost, S Hagenaaars, S C Fears, S Alonso-Lana, T G M van Erp, T Nickson, T M Chaim-Avancini, T B Meier, T Elvsåshagen, U K Haukvik, W H Lee, A H Schene, A J Lloyd, A H Young, A Nugent, A M Dale, A Pfennig, A M McIntosh, B Lafer, B T Baune, C J Ekman, C A Zarate, C E Bearden, C Henry, C Simhandl, C McDonald, C Bourne, D J Stein, D H Wolf, D M Cannon, D C Glahn, D J Veltman, E Pomarol-Clotet, E Vieta, E J Canales-Rodriguez, F G Nery, F L S Duran, G F Busatto, G Roberts, G D Pearlson, G M Goodwin, H Kugel, H C Whalley, H G Ruhe, J C Soares, J M Fullerton, J K Rybakowski, J Savitz, K T Chaim, M Fatjó-Vilas, M G Soeiro-de Souza, M P Boks, M V Zanetti, M C G Otaduy, M S Schaufelberger, M Alda, M Ingvar, M L Phillips, M J Kempton, M Bauer, M Landén, N S Lawrence, N E M van Haren, N R Horn, N B Freimer, O Gruber, P R Schofield, P B Mitchell, R S Kahn, R Lenroot, R Machado-Vieira, R A Ophoff, S Sarró, S Frangou, T D Satterthwaite, T Hajek, U Dannlowski, U F Malt, V Arolt, W F Gattaz, W C Drevets, X Caseras, I Agartz, P M Thompson, and O A Andreassen. Cortical abnormalities in bipolar disorder: an MRI analysis of 6503 individuals from the ENIGMA bipolar disorder working group. *Mol. Psychiatry*, 23(4):932–942, April 2018.

T Hinault, S Baillet, and S M Courtney. Age-related changes of deep-brain neurophysiological activity. *Cerebral Cortex*, 33(7):3960–3968, 08 2022. ISSN 1047-3211. doi: 10.1093/cercor/bhac319. URL <https://doi.org/10.1093/cercor/bhac319>.

Fengling Hu, Andrew A. Chen, Hannah Horng, Vishnu Bashyam, Christos Davatzikos, Aaron Alexander-Bloch, Mingyao Li, Haochang Shou, Theodore D. Satterthwaite, Meichen Yu, and Russell T. Shinohara. Image harmonization: A review of statistical and deep learning methods for removing batch effects and evaluation metrics for effective harmonization. *NeuroImage*, 274:120125, July 2023. ISSN 1053-8119. doi: 10.1016/j.neuroimage.2023.120125. URL <http://dx.doi.org/10.1016/j.neuroimage.2023.120125>.

Vytene Janiukstyte, Thomas W. Owen, Umair J. Chaudhary, Beate Diehl, Louis Lemieux, John S. Duncan, Jane de Tisi, Yujiang Wang, and Peter N. Taylor. Normative brain mapping using scalp eeg and potential clinical application. *Scientific Reports*, 13(1), December 2023. ISSN 2045-2322. doi: 10.1038/s41598-023-39700-7.

Jorge Jovicich, Silvester Czanner, Douglas Greve, Elizabeth Haley, Andre van der Kouwe, Randy Gollub, David Kennedy, Franz Schmitt, Gregory Brown, James MacFall, Bruce Fischl, and Anders Dale. Reliability in multi-site structural mri studies: Effects of gradient non-linearity correction on phantom and human data. *NeuroImage*, 30(2):436–443, April 2006. ISSN 1053-8119. doi: 10.1016/j.neuroimage.2005.09.046. URL <http://dx.doi.org/10.1016/j.neuroimage.2005.09.046>.

Giridhar P. Kalamangalam, Sarah Long, and Mircea I. Chelaru. A neurophysiological brain map: Spectral parameterization of the human intracranial electroencephalogram. *Clinical Neurophysiology*, 131(3):665–675, 2020. ISSN 1388-2457. doi: <https://doi.org/10.1016/j.clinph.2019.11.061>. URL <https://www.sciencedirect.com/science/article/pii/S1388245719313707>.

Anisha Keshavan, Friedemann Paul, Mona K. Beyer, Alyssa H. Zhu, Nico Papinutto, Russell T. Shinohara, William Stern, Michael Amann, Rohit Bakshi, Antje Bischof, Alessandro Carriero, Manuel Comabella, Jason C. Crane, Sandra D’Alfonso, Philippe Demaerel, Benedicte Dubois, Massimo Filippi, Vinzenz Fleischer, Bertrand Fontaine, Laura Gaetano, An Goris, Christiane Graetz, Adriane Gröger, Sergiu Groppa, David A. Hafler, Hanne F. Harbo, Bernhard Hemmer, Kesshi Jordan, Ludwig Kappos, Gina Kirkish, Sara Llufriu, Stefano Magon, Filippo Martinelli-Boneschi, Jacob L. McCauley, Xavier Montalban, Mark Mühlau, Daniel Pelletier, Pradip M. Pattany, Margaret Pericak-Vance, Isabelle Cournu-Rebeix, Maria A. Rocca, Alex Rovira, Regina Schlaeger, Albert Saiz, Till Sprenger, Alessandro Stecco, Bernard M.J. Uitdehaag, Pablo Villoslada, Mike P. Wattjes, Howard Weiner, Jens Wuerfel, Claus Zimmer, Frauke Zipp, Stephen L. Hauser, Jorge R. Oksenberg, and Roland G. Henry. Power estimation for non-standardized multisite studies. *NeuroImage*, 134:281–294, July 2016. ISSN 1053-8119. doi: 10.1016/j.neuroimage.2016.03.051. URL <http://dx.doi.org/10.1016/j.neuroimage.2016.03.051>.

SeungWook Kim, Sung-Woo Kim, Young Noh, Phil Hyu Lee, Duk L. Na, Sang Won Seo, and Joon-Kyung Seong. Harmonization of multicenter cortical thickness data by linear mixed effect model. *Frontiers in Aging Neuroscience*, 14, June 2022. ISSN 1663-4365. doi: 10.3389/fnagi.2022.869387. URL <http://dx.doi.org/10.3389/fnagi.2022.869387>.

Csaba Kozma, Gabrielle Schroeder, Tom Owen, Jane de Tisi, Andrew W. McEvoy, Anna Miserieocchi, John Duncan, Yujiang Wang, and Peter N. Taylor. Identifying epileptogenic abnormality by decomposing intracranial eeg and meg power spectra. *Journal of Neuroscience Methods*, 408:110180, August 2024. ISSN 0165-0270. doi: 10.1016/j.jneumeth.2024.110180. URL <http://dx.doi.org/10.1016/j.jneumeth.2024.110180>.

Mark A Kramer and Sydney S Cash. Epilepsy as a disorder of cortical network organization. *Neuroscientist*, 18(4):360–372, August 2012.

Naoto Kuroda, Masaki Sonoda, Makoto Miyakoshi, Hiroki Nariai, Jeong-Won Jeong, Hirotaka Motoi, Aimee F Luat, Sandeep Sood, and Eishi Asano. Objective interictal electrophysiology biomarkers optimize prediction of epilepsy surgery outcome. *Brain Commun.*, 3(2):fcab042, March 2021.

Jingwei Li, Danilo Bzdok, Jianzhong Chen, Angela Tam, Leon Qi Rong Ooi, Avram J. Holmes, Tian Ge, Kaustubh R. Patil, Mbemba Jabbi, Simon B. Eickhoff, B. T. Thomas Yeo, and Sarah Genon. Cross-ethnicity/race generalization failure of behavioral prediction from resting-state functional connectivity. *Science Advances*, 8(11), March 2022. ISSN 2375-2548. doi: 10.1126/sciadv.abj1812. URL <http://dx.doi.org/10.1126/sciadv.abj1812>.

Bethany Little, Carly Flowers, Andrew Blamire, Peter Thelwall, John-Paul Taylor, Peter Gallagher, David Andrew Cousins, and Yujiang Wang. Multivariate brain-cognition associations in euthymic bipolar disorder. *Bipolar Disord.*, 26(6):604–616, August 2024.

Kai J Miller. A library of human electrocorticographic data and analyses. *Nat. Hum. Behav.*, 3(11):1225–1235, November 2019.

Guiomar Niso, Francois Tadel, Elizabeth Bock, Martin Cousineau, Andrés Santos, and Sylvain Baillet. Brainstorm pipeline analysis of resting-state data from the open meg archive. *Frontiers in Neuroscience*, 13, 2019. ISSN 1662-453X. doi: 10.3389/fnins.2019.00284. URL <https://www.frontiersin.org/articles/10.3389/fnins.2019.00284>.

Erfan Nozari, Maxwell A. Bertolero, Jennifer Stiso, Lorenzo Caciagli, Eli J. Cornblath, Xiaosong He, Arun S. Mahadevan, George J. Pappas, and Dani S. Bassett. Macroscopic resting-state brain dynamics are best described by linear models. *Nature Biomedical Engineering*, 8(1):68–84, December 2023. ISSN 2157-846X. doi: 10.1038/s41551-023-01117-y. URL <http://dx.doi.org/10.1038/s41551-023-01117-y>.

Lauren R. Ott, Samantha H. Penhale, Brittany K. Taylor, Brandon J. Lew, Yu-Ping Wang, Vince D. Calhoun, Julia M. Stephen, and Tony W. Wilson. Spontaneous cortical meg activity undergoes unique age- and sex-related changes during the transition to adolescence. *NeuroImage*, 244:118552, 2021. ISSN 1053-8119. doi: <https://doi.org/10.1016/j.neuroimage.2021.118552>. URL <https://www.sciencedirect.com/science/article/pii/S1053811921008259>.

Thomas W. Owen, Vytene Janiukstyte, Gerard R. Hall, Jonathan J. Horsley, Andrew McEvoy, Anna Miserocchi, Jane de Tisi, John S. Duncan, Fergus Rugg-Gunn, Yujiang Wang, and Peter N. Taylor. Identifying epileptogenic abnormalities through spatial clustering of meg interictal band power. *Epilepsia Open*, 8(3):1151–1156, 2023a. doi: <https://doi.org/10.1002/epi4.12767>. URL <https://onlinelibrary.wiley.com/doi/abs/10.1002/epi4.12767>.

Thomas W. Owen, Gabrielle M. Schroeder, Vytene Janiukstyte, Gerard R. Hall, Andrew McEvoy, Anna Miserocchi, Jane de Tisi, John S. Duncan, Fergus Rugg-Gunn, Yujiang Wang, and Peter N. Taylor. Meg abnormalities and mechanisms of surgical failure in neocortical epilepsy. *Epilepsia*, 64(3):692–704, 2023b. doi: <https://doi.org/10.1111/epi.17503>. URL <https://onlinelibrary.wiley.com/doi/abs/10.1111/epi.17503>.

Genevieve Rayner and Chris Tailby. Current concepts of memory disorder in epilepsy: Edging towards a network account. *Curr. Neurol. Neurosci. Rep.*, 17(8), August 2017.

- J. A. Ricard, T. C. Parker, E. Dhamala, J. Kwasa, A. Allsop, and A. J. Holmes. Confronting racially exclusionary practices in the acquisition and analyses of neuroimaging data. *Nature Neuroscience*, 26(1):4–11, December 2022. ISSN 1546-1726. doi: 10.1038/s41593-022-01218-y. URL <http://dx.doi.org/10.1038/s41593-022-01218-y>.
- Saige Rutherford, Pieter Barkema, Ivy F Tso, Chandra Sripada, Christian F Beckmann, Henricus G Ruhe, and Andre F Marquand. Evidence for embracing normative modeling. *eLife*, 12:e85082, mar 2023. ISSN 2050-084X. doi: 10.7554/eLife.85082. URL <https://doi.org/10.7554/eLife.85082>.
- Lianne H Scholtens, Siemon C de Lange, and Martijn P van den Heuvel. Simple brain plot, 2021. URL <https://zenodo.org/record/5346593>.
- D Taussig, A Montavont, and J Isnard. Invasive EEG explorations. *Neurophysiol. Clin.*, 45(1): 113–119, March 2015.
- Delphine Taussig, Axel Lebas, Mathilde Chipaux, Maryvonne Jan, Martine Fohlen, Christine Bulteau, Nathalie Dorison, Sarah Ferrand-Sorbets, Olivier Delalande, and Georg Dorfmueller. Stereo-electroencephalography (seeg) in children surgically cured of their epilepsy. *Neurophysiologie Clinique/Clinical Neurophysiology*, 46(1):3–15, 2016. ISSN 0987-7053. doi: <https://doi.org/10.1016/j.neucli.2015.12.001>. URL <https://www.sciencedirect.com/science/article/pii/S0987705316000022>.
- Peter N Taylor, Christoforos A Papasavvas, Thomas W Owen, Gabrielle M Schroeder, Frances E Hutchings, Fahmida A Chowdhury, Beate Diehl, John S Duncan, Andrew W McEvoy, Anna Miserocchi, Jane de Tisi, Sjoerd B Vos, Matthew C Walker, and Yujiang Wang. Normative brain mapping of interictal intracranial EEG to localize epileptogenic tissue. *Brain*, 145(3): 939–949, 01 2022. ISSN 0006-8950. doi: 10.1093/brain/awab380. URL <https://doi.org/10.1093/brain/awab380>.
- Marius Tröndle, Tzvetan Popov, Andreas Pedroni, Christian Pfeiffer, Zofia Barańczuk-Turska, and Nicolas Langer. Decomposing age effects in eeg alpha power. *Cortex*, 161:116–144, April

2023. ISSN 0010-9452. doi: 10.1016/j.cortex.2023.02.002. URL <http://dx.doi.org/10.1016/j.cortex.2023.02.002>.

Christopher Turner, Satu Baylan, Martina Bracco, Gabriela Cruz, Simon Hanzal, Marine Keime, Isaac Kuye, Deborah McNeill, Zika Ng, Mircea van der Plas, Manuela Ruzzoli, Gregor Thut, Jelena Trajkovic, Domenica Veniero, Sarah P Wale, Sarah Whear, and Gemma Learmonth. Developmental changes in individual alpha frequency: Recording EEG data during public engagement events. *Imaging Neurosci (Camb)*, 1:1–14, August 2023.

Yujiang Wang, Nishant Sinha, Gabrielle M Schroeder, Sriharsha Ramaraju, Andrew W McEvoy, Anna Miserocchi, Jane de Tisi, Fahmida A Chowdhury, Beate Diehl, John S Duncan, et al. Interictal intracranial electroencephalography for predicting surgical success: The importance of space and time. *Epilepsia*, 61(7):1417–1426, 2020.

Yujiang Wang, Gabrielle M. Schroeder, Jonathan J. Horsley, Mariella Panagiotopoulou, Fahmida A. Chowdhury, Beate Diehl, John S. Duncan, Andrew W. McEvoy, Anna Miserocchi, Jane de Tisi, and Peter N. Taylor. Temporal stability of intracranial electroencephalographic abnormality maps for localizing epileptogenic tissue. *Epilepsia*, 64(8):2070–2080, 2023. doi: <https://doi.org/10.1111/epi.17663>. URL <https://onlinelibrary.wiley.com/doi/abs/10.1111/epi.17663>.

Brady T. West, Kathleen B. Welch, and Andrzej T Galecki. *Linear Mixed Models: A Practical Guide Using Statistical Software, Second Edition*. Chapman and Hall/CRC, July 2014. ISBN 9780429186561. doi: 10.1201/b17198. URL <http://dx.doi.org/10.1201/b17198>.

Thomas J. Whitford, Christopher J. Rennie, Stuart M. Grieve, C. Richard Clark, Evian Gordon, and Leanne M. Williams. Brain maturation in adolescence: Concurrent changes in neuroanatomy and neurophysiology. *Human Brain Mapping*, 28(3):228–237, February 2007. ISSN 1097-0193. doi: 10.1002/hbm.20273. URL <http://dx.doi.org/10.1002/hbm.20273>.

W J E M Zweiphenning, M A van ‘t Klooster, E van Diessen, N E C van Klink, G J M Huiskamp, T A Gebbink, F S S Leijten, P H Gosselaar, W M Otte, C J Stam, K P J Braun, and G J M

Zijlmans. High frequency oscillations and high frequency functional network characteristics in the intraoperative electrocorticogram in epilepsy. *NeuroImage Clin.*, 12:928–939, February 2016.

Willemieck J E M Zweiphenning, Hanneke M Keijzer, Eric van Diessen, Maryse A van 't Klooster, Nicole E C van Klink, Frans S S Leijten, Peter C van Rijen, Michel J A M van Putten, Kees P J Braun, and Maeike Zijlmans. Increased gamma and decreased fast ripple connections of epileptic tissue: A high-frequency directed network approach. *Epilepsia*, 60(9):1908–1920, September 2019.